



JGR Atmospheres

RESEARCH ARTICLE

10.1029/2025JD044574

Key Points:

- Building-resolved modeling of tornado-like vortex (TLV) shows significant dynamic impact of buildings on TLV-associated local strong winds
- When TLV passes a building cluster, its low-level structures are blocked by buildings, while its upper part merges with building-lee vortex
- TLV may re-intensify with an elongated corridor of local strong winds in the open area between building clusters

Supporting Information:

Supporting Information may be found in the online version of this article.

Correspondence to:

G. Chen and L. Bai, chenguixing@mail.sysu.edu.cn; bailanqiang@foxmail.com

Citation:

Kong, X., Chen, G., Bai, L., Ran, L., Zhang, S., & Meng, Z. (2025). A mesoscale-to-LES modeling of tornado-like vortex and associated local strong winds in urban area. *Journal of Geophysical Research: Atmospheres*, 130, e2025JD044574. https://doi.org/10.1029/ 2025JD044574

Received 14 JUN 2025 Accepted 29 AUG 2025

Author Contributions:

Conceptualization: Xiangrui Kong Formal analysis: Xiangrui Kong Funding acquisition: Guixing Chen, Lingkun Ran, Zhiyong Meng Methodology: Xiangrui Kong Project administration: Guixing Chen Resources: Lanqiang Bai, Lingkun Ran,

Shaoting Zhang
Software: Guixing Chen
Supervision: Guixing Chen
Validation: Lanqiang Bai
Visualization: Xiangrui Kong
Writing – original draft: Xiangrui Kong

Writing – review & editing: Guixing Chen, Lanqiang Bai, Lingkun Ran, Shaoting Zhang,

Zhiyong Meng

© 2025. American Geophysical Union. All Rights Reserved.

A Mesoscale-to-LES Modeling of Tornado-Like Vortex and Associated Local Strong Winds in Urban Area

Xiangrui Kong¹, Guixing Chen¹, Lanqiang Bai², Lingkun Ran³, Shaoting Zhang⁴, and Zhiyong Meng⁵

¹Southern Marine Science and Engineering Guangdong Laboratory (Zhuhai), Guangdong Province Key Laboratory for Climate Change and Natural Disaster Studies, School of Atmospheric Sciences, Sun Yat-sen University, Zhuhai, China, ²China Meteorological Administration Tornado Key Laboratory, Foshan Tornado Research Center, Guangdong Meteorological Service, Foshan, China, ³Institute of Atmospheric Physics, Chinese Academy of Sciences, Beijing, China, ⁴Sanshui Meteorological Service, Foshan, China, ⁵China Meteorological Administration Tornado Key Laboratory, Department of Atmospheric and Oceanic Sciences, School of Physics, Peking University, Beijing, China

Abstract Tornadoes in urban areas pose a great threat to local residents and buildings. The tornado's fine-scale dynamic structures in turn can be disturbed by these buildings. This study employs an advanced modeling system of mesoscale-to-large eddy simulation (LES) to explicitly resolve both the tornado-like vortex (TLV) and building-induced flow disturbances. Our modeling reasonably reproduced a TLV passing over building clusters, while the evolutionary characteristics of TLV are comparable to that of the video-captured tornado funnels of an actual event in South China. The structures of the TLV are significantly disturbed as it approaches high-rise building clusters. After arriving at the downstream of the building cluster, the disturbed TLV regains a well-defined structure. Such a reconstruction of TLV structures is characterized by the vertical alignment of the original aloft TLV structures and low-level building-induced lee vortex. As the TLV detaches the building cluster, it leaves open space for a wind corridor, a band area of high wind speeds along the direction of ambient flow in the open area among building clusters. This corridor delivers momentum that, when coupled with the reconstruction of TLV, favors local strong winds. Such a type of local strong winds are highly related to the heights of building clusters but are somewhat less sensitive to the detailed TLV track relative to building clusters, as indicated by numerical sensitivity experiments. These results provide insight into possible wind speed changes when tornadoes encounter buildings, which may have valuable implications for urban wind hazard mitigation.

Plain Language Summary As tornadoes hit urban areas, some visual evidence indicates that the tornadoes' funnel clouds are disturbed by high-rise building clusters. Such impressive scenes suggest the possible interactions between tornadic flows and building-induced flow disturbances. Using a state-of-the-art modeling system, this study conducts a series of super-high-resolution simulations to reproduce the passing of a tornado-like vortex (TLV) across high-rise building clusters. Results show that the TLV main vortex is disturbed by the blocking of building clusters ahead and then it is reorganized with building-lee vortices. Afterward, the TLV main vortex re-intensifies as it moves into an open area, where local strong winds are favored by a wind corridor formed between building clusters. We also note that the evolution of TLV structures among buildings and associated variations of local strong winds appear somewhat related to building geometries, as indicated by sensitivity experiments. These findings may be helpful for the risk assessment of urban wind hazards.

1. Introduction

Tornadoes sometimes strike urban areas (e.g., Bai et al., 2017; Dunn & Vasiloff, 2001; Edwards & Schaefer, 2025; Zhang et al., 2020), which can bring severe damage to buildings and cause a large sum of casualties and property loss. With the expansion of urban areas, the exposure of cities to tornado hazards may increase (Ashley et al., 2014; Cusack, 2014). Some studies have evaluated tornadoes' damage to buildings from an engineering perspective (e.g., Badmus & Sutley, 2025; Huang et al., 2016). Such evaluation helps to rate the intensity of tornadoes (e.g., Marshall, 2002; Wurman & Alexander, 2005). On the other hand, dense buildings in urban areas are noted to disturb the fine-scale dynamic structures of a tornado (Kawaguchi et al., 2019, 2020). Further improving the understanding of tornadoes and their associated strong winds affected by buildings may benefit urban wind hazard mitigation.

KONG ET AL. 1 of 23

In urban areas, the heterogeneity of surface conditions leads to complex dynamic disturbances and thermal turbulences, which affect local winds (e.g., Du et al., 2022; L. Li et al., 2021). To isolate the effects of urban surface on flows, most studies employ idealized inflow conditions (e.g., Inagaki et al., 2017; Mo et al., 2021; Wang & Ng, 2018). These studies have elucidated wind patterns over varying urban morphologies and background flows (Mittal et al., 2018; Oke et al., 2017). However, realistic weather usually exhibits inhomogeneity due to small-scale disturbances, and sometimes even sharp gradients of meteorological fields. Some studies have focused on the interaction of urban surfaces and background weather systems such as tropical cyclones (Takemi et al., 2019, 2020), sea breeze (Chen et al., 2019) and synoptic frontal passages (Bornstein & Thompson, 1981). Though tornadoes have varying horizontal scales, their typical diameters are on the order of 100 m (Markowski & Richardson, 2010). When tornadoes are affected by buildings with similar horizontal scales, more distinctive fine-scale structures may form compared to other larger-scale weather systems.

Tornadoes have intrinsic fine-scale structures, which far exceed the complexity of a smooth pattern of cyclonic vortex. These fine-scale structures have been revealed through high-resolution observations by rapid-scanning Doppler radar on wheels (e.g., Pazmany et al., 2013). For instance, the multiple wind maxima, and the multivortices revolving about surface tornadic circulations have been reported (Wurman & Gill, 2000; Wurman et al., 2014). Kosiba et al. (2008) presented that the evolution of tornadic dynamic structures in the boundary layer is associated with the near-surface wind speeds. Damage surveys of fields also showed evidence on the asymmetric distribution of wind speeds in tornadic vortices (e.g., Beck & Dotzek, 2010; Fujita et al., 1972). The fine-scale structures of tornadoes can be modulated by surrounding conditions, such as background convective systems (e.g., Yao et al., 2019), terrain and surface roughness (e.g., Lewellen, 2012; Satrio et al., 2020). In an urban case, damage surveys showed the changing intensity of a tornado when passing over different types of built-up areas (Zhang et al., 2020), suggesting that the building-induced disturbances on tornado structures may affect urban local strong winds. Therefore, it's worth examining the fine-scale structures of tornadoes that evolve over urban areas and their relationship with local strong winds.

Due to the difficulties in observation especially in urban areas, laboratory or numerical simulations are utilized to reproduce finer 3-D dynamic structures of tornadoes and their evolution. Fiedler (1998) conducted an idealized numerical simulation of tornado and obtained multiple suction vortices inside the main cyclone, which were similar to that in observations. Using a tornado simulator and a scaled building, Yang et al. (2011) obtained the characteristics of building-lee vortices in tornado-like winds, such as the inclination of the positive building-lee vortex toward the tornado-like vortex (TLV). Through idealized numerical experiments, Gorecki and Selvam (2013) demonstrated that when an idealized tornadic vortex passed over an idealized building, it split a vortex tip in the downstream of the building. They also conducted sensitivity experiments and found that higher building leads to more extended sheltering regions with low wind speeds. For the effects of more buildings, Lewellen (2014) showed that when a tornado passes over blocks of buildings, it is weakened at first and reintensified afterward. Most previous modeling studies on urban tornadoes are based on idealized tornado-like vortices. If the realistic conditions of both tornadoes and buildings are introduced, the situation may become more complex.

To explicitly resolve both realistic weather system and building-induced disturbances above a city, "mesoscale-to-LES" modeling system has been adopted, which downscales the outputs from a mesoscale model to a CFD model with large-eddy simulation (LES) scheme (e.g., Chen et al., 2015; Muñoz-Esparza et al., 2021; Nakayama et al., 2012; Park et al., 2015). This kind of modeling system has been successfully used in urban meteorology studies under various disastrous wind backgrounds such as cold surge and typhoon (Takemi et al., 2019; Xiang et al., 2019). Recently, Kawaguchi et al. (2019, 2020) have applied a mesoscale-to-LES modeling system to study the impacts of buildings on tornadoes. The modeling results in Kawaguchi et al. (2020) were validated with damage surveys, demonstrating the potential of the modeling system to reproduce realistic tornadoes in densely built-up urban areas. Some fine-scale structures of meteorological fields under the impacts of buildings are described, such as the strong vertical vortices at the corners of buildings which stretched upward and merged with the main structure of the tornado (Kawaguchi et al., 2019). In their simulation of a real tornado case, the underlying buildings were below 30 m (Kawaguchi et al., 2020). However, tornadoes used to pass over high-rise buildings near 100 m, such as in downtown Salt Lake City, USA and Foshan, China (Bai et al., 2017; Dunn & Vasiloff, 2001). The impact of high-rise building (clusters) on tornado structures and associated local winds is worthy of further study.

KONG ET AL. 2 of 23

In this study, we use the building-resolved mesoscale-to-LES modeling system to simulate a real tornado passing through a built-up area, and a TLV is obtained. We aim to investigate how the fine-scale structures of the tornado and associated local strong winds are affected by realistic high-rise buildings. This article is organized as follows. In Section 2, the tornado case and settings of the mesoscale-to-LES modeling system are introduced. In Section 3, the modeling results in different scales are examined. In Section 4, the simulated TLV structures under their interaction with building-induced vortices are investigated, and the attendant local strong winds are also examined. In Section 5, the sensitivity of TLV structures and associated local strong winds to buildings' configurations is discussed. A summary is provided in Section 6.

2. Data and Methods

2.1. Data

The tornado of interest that struck the urban area of Foshan, a highly urbanized coastal city in southern China, occurred on the afternoon of 4 October 2015. It was spawned by a miniature supercell embedded in a tropical cyclone rainband during 15:28–16:00 LST (Figure 1a). Post-event damage surveys confirmed an EF3 rating on the enhanced Fujita scale, leaving 4 fatalities and hundreds of injuries (Bai et al., 2017). Located approximately 350 km from the center of Typhoon Mujigae, the tornado tracked northwestward within the typhoon's ambient southeasterlies (Figures 1a and 1b). In this study, three kinds of observations on the tornado are used to demonstrate its characteristics, which are compared with simulated TLV's characteristics.

First, data from the operational S-band Doppler radar in Guangzhou (\sim 24 km to the northeast of the tornado's track) are used to be compared with the mesoscale modeling results from supercell scale to a coarse tornadic scale (Figures 1b and 1c). In the supercell-scale observation of reflectivity, the miniature supercell was characterized by a hook echo (Figure 1b). The tornado was born at the tip of the hook echo at around 15:28–16:00 LST, and its track aligned closely with the movement of the "hook." In the coarse tornadic-scale observation of radial velocities at 15:36 LST (Figure 1c), a tornado vortex signature (TVS; American Meteorological Society, 2012) with a gate-to-gate change from negative to positive velocities was caught at near 420 m above ground level. The TVS reached about 60 m s⁻¹, within the scale of one beamwidth of only 400 m (Bai et al., 2017). The EF0 damage swath of the tornado case on the ground passed by the northeast of the TVS, indicating that the observed TVS was related to the tornado.

Second, a video taken by an amateur eyewitness at 15:32–15:34 LST, which captured the tornado of our case passing through the built-up area, is used in our study. This video roughly shows that the tornado vortex was blocked and re-established when passing over a building cluster, and such tornado's evolutionary characteristics are compared with that shown by the wind fields of the simulated TLV in Section 4.2.

Finally, a damage map from Bai et al. (2017) derived from damage surveys is further analyzed. This damage map (Figure 3 in Bai et al. (2017)) shows that the approximate track of the tornado indeed passed through the building cluster captured in the video. Also, it marks the damage intensity of the real tornado near the building cluster, which is compared with the evolution of TLV's intensity when passing over building clusters (Section 4.2). For the integrated damage, visual and professional meteorological observation analysis of the tornado case in more detail, the studies by Bai et al. (2017) and Zhao et al. (2017) can be referred to.

2.2. Mesoscale-to-LES Modeling System

To reproduce the fine-scale structures of tornadoes in urban areas, we use a mesoscale-to-LES modeling system in which the mesoscale modeling results are one-way nested to a CFD model with LES scheme (Chen et al., 2015). The mesoscale model is used to produce realistic atmospheric background conditions and convective systems. The CFD model is used to explicitly resolve individual buildings in the inner domain over the city. In the first stage of our modeling, the Advanced Research WRF model version 3.9 is used as the mesoscale model (Skamarock et al., 2008). A 24-hr simulation since 08:00 LST 4 October 2015, when the tornado case occurred, is conducted with a highest horizontal grid spacing of 148 m. The main settings of the WRF simulation are presented in Table 1, which are the same as those used by Tang et al. (2019).

In the second stage of our mesoscale-to-LES modeling, the outputs from the innermost domain of the mesoscale model are used as initial and boundary conditions to drive the CFD model in a city domain. A CFD model that explicitly resolves steep terrain and urban buildings in 3-D Cartesian coordinates is used in our study, in which

KONG ET AL. 3 of 23

21698996, 2025, 17, Downloaded from https://agupubs.onlinelibrary.wiley.com/doi/10.1029/2025ID044574 by Peking University Health, Wiley Online Library on [25/09/2025]. See the Terms and Conditions

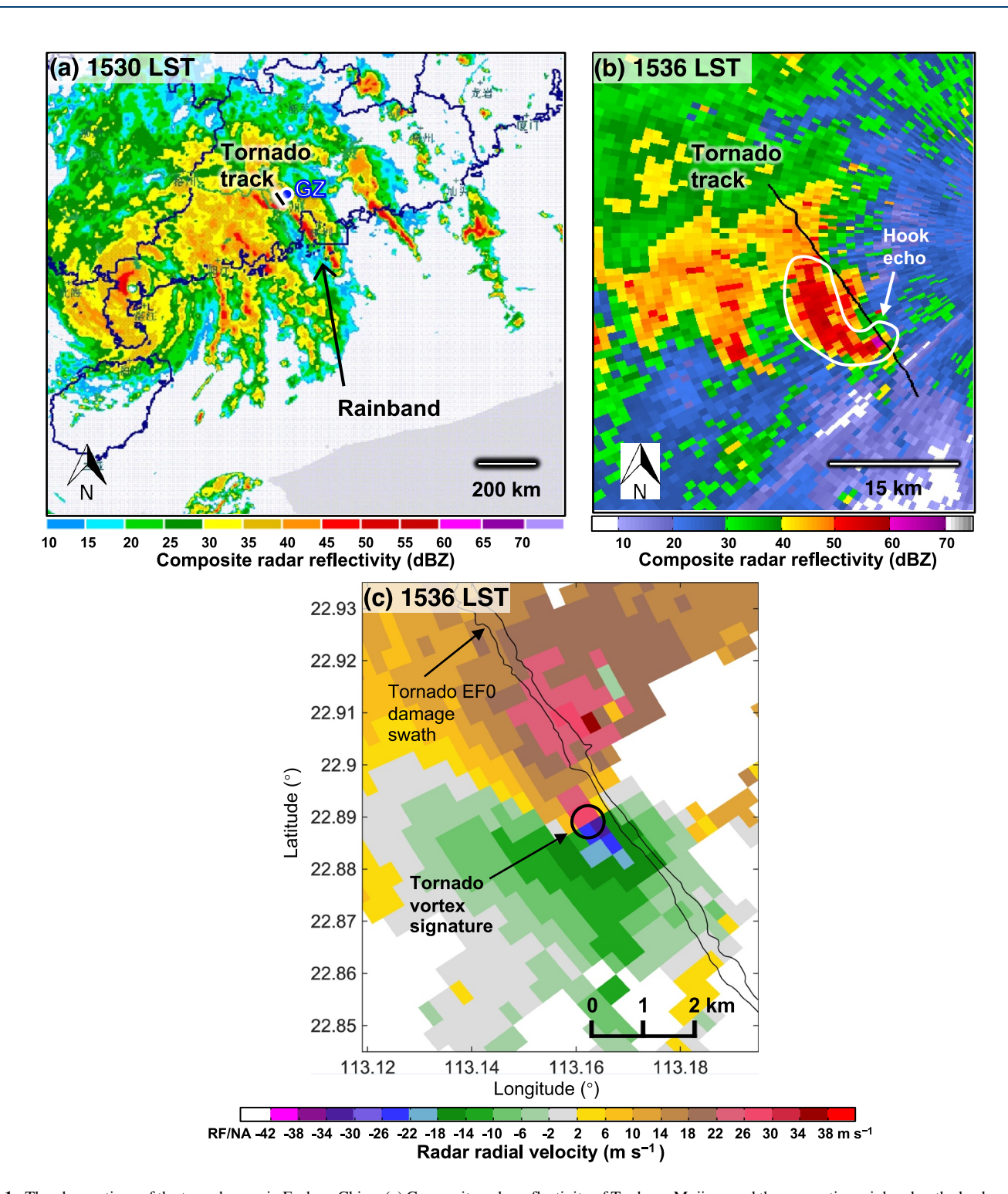


Figure 1. The observations of the tornado case in Foshan, China. (a) Composite radar reflectivity of Typhoon Mujigae and the convective rainband as the background of the tornado at 15:30 LST 4 October 2015. The tornado track (black line) and the location of the Guangzhou (GZ) Doppler radar (blue dot) is shown. (b) Radar reflectivity of the background miniature supercell of the tornado at 15:36 LST 4 October 2015. The tornado track is shown with a black curve and the hook echo is marked with a white curve. (c) Radar radial velocities of the mesocyclone where the tornado was born at the same time of (b), while the missing velocities are represented by white shadings. The location of the tornado vortex signature (black circle) and the tornado's EFO damage swath (black contours) derived from the damage survey of Bai et al. (2017) are shown. The radar data of panels (b) and (c) are from the 0.5° scans of the Guangzhou radar.

KONG ET AL. 4 of 23

21698996, 2025, 17, Downloaded from https://agupubs.onlinelibrary.wiley.com/doi/10.1029/2025JD044574 by Peking University Health, Wiley Online Library on [25/09/2025]. See the Terms

Table 1
Summary of Settings Used in Mesoscale-to-LES Modeling System

	WRF				
Models and domains	d01	d02	d03	d04	SIMPLERgo
Horizontal grid spacing	4,000 m	1,333 m	444 m	148 m	6 m
Horizontal grids	$1,500 \times 1,100$	800×690	800×690	960×600	$1,744 \times 1,744$
Vertical grid spacing	-	-	-	-	6-10 m stretched
Vertical grids	51	51	51	51	220
Model top	50 hPa	50 hPa	50 hPa	50 hPa	3126.9 m
Calculation timestep	9 s	3 s	1 s	0.33 s	0.25 s
Output interval	30 min	60 min	30 min	5 min	1 s
Microphysics	Morrison 2-moment				None
Cumulus	None				None
Radiation	CAM (Community Atmosphere Model)				None
Planetary boundary layer	ACM2 (Asymmetric Convective Model with non-local upward mixing and local downward mixing)				LES
Land surface	Pleim-Xiu land surface model				None
Urban canopy	None				None

Lilly–Smagorinsky LES model is utilized for the parameterization of sub-grid eddies (Lilly, 1962; Smagorinsky, 1963). The model based on the fully compressible Navier-Stokes equations is called SIMPLERgo (Chen et al., 2015; Sha, 2002, 2008), named after an algorithm of the Semi-Implicit Method for Pressure-Linked Equation Revised code (Patankar, 1980, pp. 131–134). Such an algorithm can instantly reconstruct pressure deviations around obstacles, thereby rapidly generating wind perturbations at the beginning of simulation. The parallelized version of this CFD model accommodates both idealized and realistic, meso- and micro-scale weather forcing over a mega-city domain at meter-scale resolution. The dynamic impact of buildings is resolved with a blocking-off method (Patankar, 1980, pp. 147–149), in which the obstacle shape is approximated by full grid cells to fit the grid and a grid is either 100% fluid or 100% obstacle. Then, if a grid is marked as an obstacle, it becomes inactive and the velocity must be set to zero. The third-order upwind Quadratic Upstream Interpolation for Convective Kinematics (QUICK) scheme is used for advection (Leonard, 1979). For the lateral and upper boundaries, an improved Orlanski-type radiation condition is used to get rid of the reflection of gravity wave propagation (Orlanski, 1976). The no-slip boundary condition is used as the lower boundary condition.

Previous studies have demonstrated that this CFD model can simulate well the fine-scale structures of horizontal convective rolls, sea breeze and cold surge above urban areas (Chen et al., 2015, 2019; Xiang et al., 2019). These simulated fine-scale structures correspond well with the observations of ground-based automatic weather stations, heliborne sensors and high-resolution lidar. In our study, due to the lack of quantitative meteorological observations of tornado at the scale of meters, videos caught by camera are used to be compared with the CFD modeling results (Section 4.2), following the approach of Bai et al. (2017) and Oliveira et al. (2019).

Grids and static geographic data of the CFD model are set as follows and Table 1. The horizontal range of the CFD domain is 10,464 m × 10,464 m (Figure 2d), with grid spacing of $\Delta X = \Delta Y = 6$ m. The building height data of Foshan in 2018 are derived from a map service provider of China, A-map (https://amap.com), and the terrain elevation data of MERIT-DEM (Yamazaki et al., 2017) are loaded into the domain. A buffer zone of 500 m wide without buildings is applied to lateral boundary areas. The vertical grid spacing is $\Delta Z = 6$ m up to Z = 360 m above sea level (ASL), and then it increases with a stretch ratio of 1.08 until Z = 516.9 m ASL. Above this height, a uniform vertical grid spacing of $\Delta Z = 10$ m is used until Z = 3126.9 m ASL, which is the top of the CFD domain.

The initial and boundary conditions (including meteorological and surface conditions) of the CFD model in the control run (CTL) are described below. The outputs from the mesoscale model including three-dimensional wind, potential temperature and pressure fields at single timestep (15:55 LST 4 October 2015) are one-way nested to the CFD domain. At this timestep, the vertical vorticity of the TLV develops the most pronounced in WRF. They are

KONG ET AL. 5 of 23

21698996, 2025, 17, Downloaded from https://agupubs.onlinelibrary.wiley.com/doi/10.1029/2025JD044574 by Peking University Health, Wiley Online Library on [25/09/2025]. See the Terms and Conditions (https://onlinelibrary.wiley

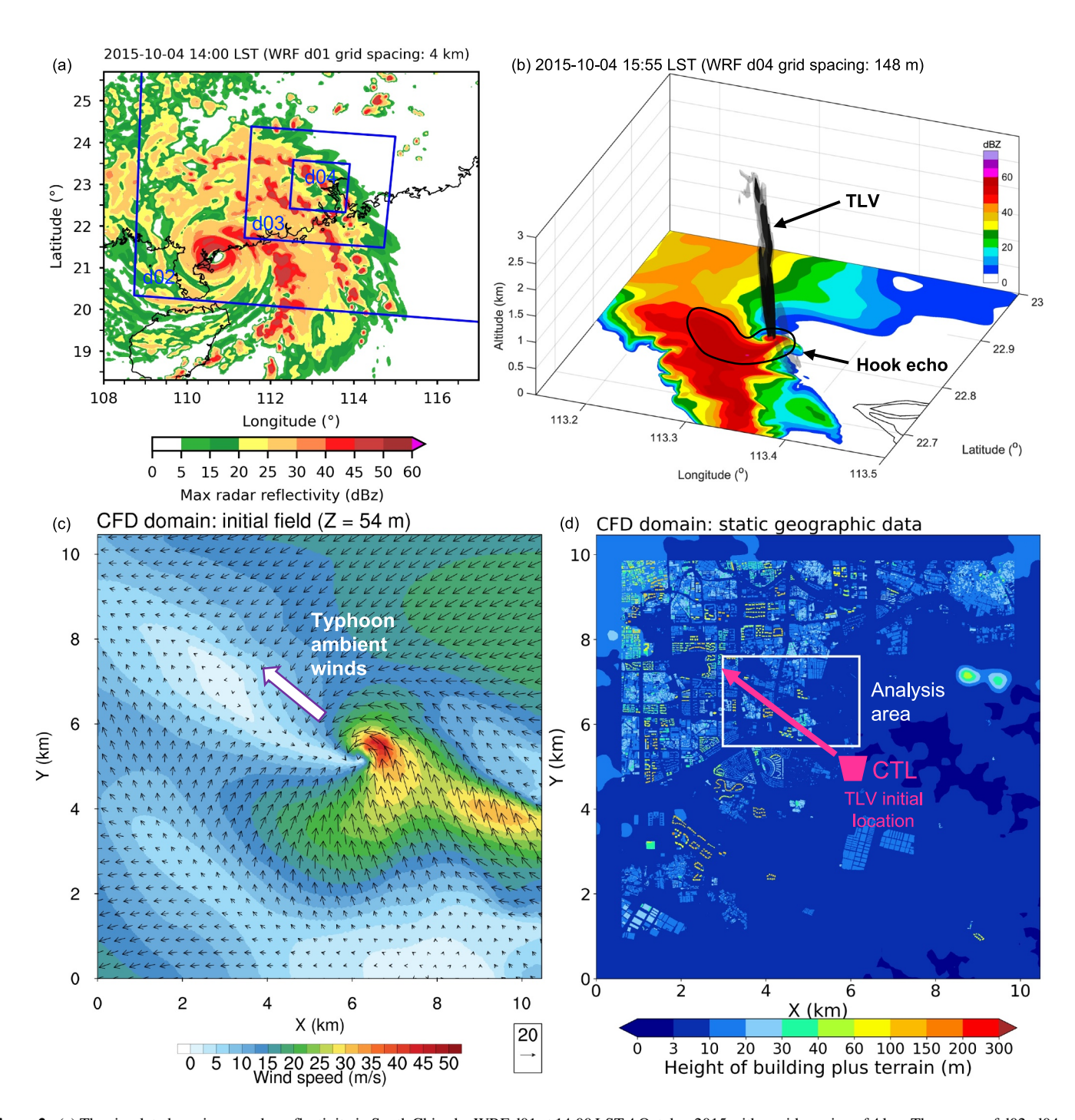


Figure 2. (a) The simulated maximum radar reflectivity in South China by WRF d01 at 14:00 LST 4 October 2015 with a grid spacing of 4 km. The ranges of d02–d04 are marked with blue rectangles. (b) The simulated radar reflectivity (shading) of miniature supercell and 3-D vertical vorticity (the gray and black isosurfaces represent 0.05 and 0.06 s^{-1} , respectively) simulated by WRF d04 at 15:55 LST 4 October 2015 with a grid spacing of 148 m. The hook echo is marked with black curve. (c) The initial wind field of the CFD model at Z = 54 m above sea level. (d) The height of building plus terrain (m) in the CFD domain for CTL run. The magenta trapezoid and line with an arrow represent the initial location and approximate track of the tornado-like vortex for CTL run, respectively. The analysis area of CTL run is marked with white rectangle.

linearly interpolated to the desired grid spacing and become the initial and boundary conditions of the CFD model. The WRF-simulated average surface temperature in the geographical range of the CFD domain is set as the uniform ground and wall temperature in the CFD model, which does not change with time. The real tornado started over an open area. Then its track passed through one high-rise building cluster located approximately

KONG ET AL. 6 of 23

2.7 km northwest of the initial location of the TLV, where the surrounding buildings are sparse (see Figure 3 in Bai et al. (2017)). To reproduce the realistic process that the TLV passes over a building cluster, and also investigate the possible impact of following more building clusters on the TLV, we adjust the settings of modeling as follows. In the CFD domain shown in Figure 2d, we manually set the initial location of the TLV (marked with trapezoid) to an open nursery in the southeast of downtown Foshan, so that the TLV will move northwestward to the area with dense high-rise buildings under the guidance of ambient southeasterlies. The CFD model is run for 211 s with a timestep of 0.25 s. A shorter timestep has been tried (e.g., 0.1 s), while the modeling results of wind fields is rather similar to the run with the original timestep. Since the CFD model is not spun up with turbulence and the integration time prior to the TLV encountering buildings is limited, it should be noted that the simulated flow in the upstream regions of buildings is quite laminar, falling short of the realistic turbulent features.

To further examine the impact of the heights and configurations of buildings on TLV structures and related local strong winds, we conduct four numerical sensitivity experiments besides CTL. For the impact of building heights, the experiments halving the heights of all buildings (0.5H_BLD) and removing all buildings (NO_BLD) are conducted, and NO_BLD is regarded as a baseline experiment. For the impact of slight shift of buildings' configurations, experiments shifting the topography including buildings southward or northward both by 250 m (BLD_S and BLD_N, respectively) are conducted.

3. Overview of Modeling Results

In this section, the mesoscale modeling results are analyzed at different scales, and the outputs from the CFD model inside the urban domain are briefly checked. Figure 2a shows the simulated maximum radar reflectivity in "d01" of WRF before the tornado occurred. The WRF simulation is found to reproduce well the general patterns and convective systems of Typhoon Mujigae. Specifically, the rainbands with active convection with reflectivity of over 45 dBZ are mainly located to the east sector of the typhoon, which are consistent with the observed ones (cf., Figures 1a and 2a). At storm scale, a well-defined hook echo (marked with a black curve in Figure 2b) is reproduced in the supercell that develops in the innermost WRF domain over Foshan between 15 and 16 LST. A column of large vertical vorticity (greater than $0.06 \, {\rm s}^{-1}$) is located on the hook echo, indicating the simulated tornado-related vortex. This simulated vortex is regarded as a TLV, since the spatial grid spacing of 148 m is relatively coarse compared to the realistic structures of tornadoes (J. Li et al., 2022), as the diameter of the real tornado's condensation funnel (CF) at the ground is only about 13.3 m measured through a video in this case (Bai et al., 2017). The TLV shows a northwestward track along with the hook echo. These features agree well with the radar observation, despite a spatial bias of about 13 km northwest and a temporal slow bias of approximately 30 min. Given that the WRF model reproduces well both the typhoon's rainbands and the TLV-related miniature supercell, the atmospheric conditions of the real tornado might be faithfully provided.

Figure 2c shows the "d04" modeling results of a near-surface wind field at 15:55 LST. Near the center of Figure 2c, the high speeds of about 50 m s⁻¹ (EF2 level) are identified near the cyclonic flow pattern, which corresponds to the TLV in Figure 2b. The extreme winds are mainly localized in the north and east quadrant of the TLV, which shape a comma-like asymmetric pattern of high speeds similar to the observed TLV. Such an asymmetric wind speed pattern is attributed to the overlapping ambient winds brought by the typhoon, and it is also recorded in the tornado damage map by Bai et al. (2017). Because of the relatively coarse resolution of WRF, considerable distance between TLV's strong wind quadrant and TLV's center is shown (Figure 2c, also Figure 3c), while the velocity feature of the TVS with a scale smaller than 400 m is not caught. Also, the coarse resolution might cause the discrepancy of the simulated maximum wind speeds (EF2 level) and the real ones (causing EF3-level damage), as Zhu and Zhao (2022) simulated a stronger TLV when the model's grid spacing was improved from 250 to 75 m. In general, the realistic meteorological fields of the tornado case are successfully reproduced from synoptic scale to tornado-like scale, which firmly support the following CFD modeling.

In the stage of CFD modeling, the evolution of general wind patterns in CTL at Z = 54 m ASL (near half of the height for most buildings in the domain) are presented in Figure 3. At the forecast time of 40 s (FCST = 40 s), in the center of the CFD domain, the model has produced a hook-like pattern of high wind speeds, characterized by strong southerlies in the east of the TLV, and relatively narrow zone of strong easterlies and northeasterlies in the north (Figure 3a, also in Figure 3b for zooming in). Such a hook-like pattern looks more like an annulus of an idealized vortex, and is evolved and refined from the comma-like pattern in the initial field from WRF (Figure 3c). As measured, the radius of maximum winds of the TLV reduces from about 620 m in WRF, to about 374 m in the

KONG ET AL. 7 of 23

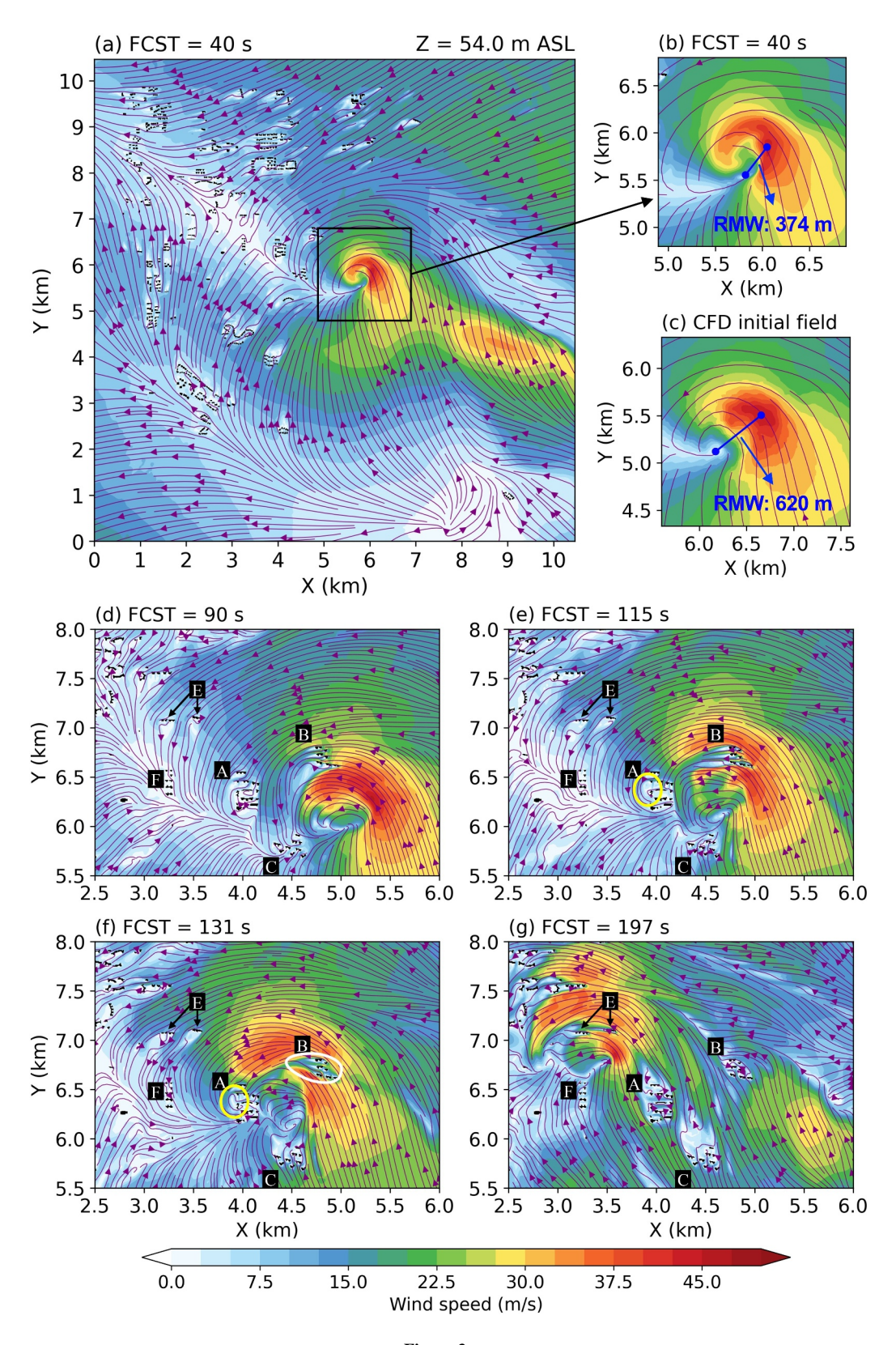


Figure 3.

KONG ET AL. 8 of 23 CFD model (cf., Figures 3b and 3c). These characteristics show the revisions of the high-resolution CFD model in the aspect of TLV's horizontal winds. Both patterns have similar maximum wind speeds of over 42.5 m s⁻¹, which does not show systematic wind speed decay after being transferred to CFD stage. At this timestep, in the north of the CFD domain (Figure 3a), low horizontal wind speeds are seen downwind from the dense buildings. All above features indicate that the meter-scale CFD model can reliably simulate the local winds including both the hook-like pattern of TLV and building-induced eddies.

At FCST = 90 s, the northwestward moving TLV starts to be affected by high-rise buildings (Figure 3d). The easterlies or northeasterlies at the north sector of the TLV are partly blocked by building cluster "B," and the wake of low horizontal wind speeds is generated. At FCST = 115 s, the hook-like strong wind pattern of TLV is divided into two parts at both north and south flanks of "B" (Figure 3e). Such a feature indicates that the typical pattern of flow acceleration along the flanks of an obstacle (Hussein & Martinuzzi, 1996; Larousse et al., 1993; Oke et al., 2017) is also applied to the condition where the background flow is induced by small-scale TLV. At the west downwind area of building cluster "A," a local vortex is indicated by streamlines. Such a building-lee vortex is thought to be generated by the horizontal wind shear between the wake and flanks of the building cluster, which can be seen in the laboratory experiment in tornado-like flow (Yang et al., 2011).

At FCST = 131 s, when the north sector of the TLV passes over building cluster "B," the divided strong wind pattern around "B" merges downstream, leading to a more confined low-speed wake (Figure 3f). Finally, at FCST = 197 s, as the TLV continues moving northwestward to the downstream urban area with more complexly distributed building clusters, its strong winds are once more divided into several local speed maxima (Figure 3g). Now the wind pattern of TLV has become remarkably complicated as it is disturbed by buildings, which is significantly different from the smooth pattern at earlier timesteps (cf., Figures 3b and 3g).

4. Fine-Scale Structures and Associated Winds of TLV in Urban Area

4.1. Three Types of Local Strong Winds Associated With TLV

In this section, we further investigate different types of local strong winds associated with TLV and their relationships with buildings. Figure 4 shows the spatial patterns of composite maximum horizontal wind speeds and maximum vertical motions over the whole CTL run. The wind directions at the timesteps with peak wind speed for each grid are shown by vector. As wind maxima might be derived from different timesteps, even in adjacent grids the associated wind directions can greatly differ, leading to discontinuous interfaces of plotted wind vectors. Such discontinuous interfaces show that the strong winds might occur in different sectors of TLV's wind patterns, which help to clarify the probable causes. The differences of maximum horizontal wind speeds between CTL and NO_BLD, as well as CTL and 0.5H_BLD are shown in Figure 5. Based on different patterns of wind speeds, directions, or the differences of maximum wind speeds between building sensitivity experiments, we can classify the TLV-associated local strong winds into three types.

At $Z=54\,\mathrm{m}$ ASL, as marked with a black curve in Figure 4c, the region of strong winds occurring to the southeast of building cluster "B" are referred to as "Type 1." In the upstream open area of building cluster "B," they have not been disturbed by high-rise buildings, so they are the strongest winds during the entire TLV impact period. Their impact range with a width of over 500 m, extends northwestward parallel to the TLV track. Their large-scale continuous southerlies to southeasterlies originate from the TLV's northeast quadrant, as evident in the hook-like pattern of strong wind speeds (Figure 3b). These features indicate that Type 1 are caused by the TLV itself superimposing on the ambient flow by typhoon, which can be reproduced well by mesoscale weather models such as WRF (e.g., Yao et al., 2019). In our previous WRF simulation, the coarse grid spacing affects the model's capability to represent the TLV. Then, due to the translation effects of the model from coarse to fine grid spacings,

Figure 3. Instantaneous horizontal wind fields for typical timesteps during the CTL run at the plane of Z = 54 m above sea level. Shading represents horizontal wind speeds, and purple streamlines indicate wind directions. Buildings above the plotting plane are shown in black. Different high-rise building clusters are marked with white capital letters inside black boxes. (a) At CFD forecast time (FCST) of 40 s, and the plotting area is the whole CFD domain. (b) Zoom in on the tornado-like vortex (TLV). (c)–(g) Same as (b), but for the initial field of the CFD model or at FCST = 90, 115, 131, and 197 s, respectively. In panels (b) and (c), the blue terminated lines with rounded endpoints mark the radius of maximum winds (RMW) of the TLV. The white oval region in panel (f) marks the low-wind-speed area of the building wake. Yellow circles in panels (e) and (f) mark the lee vortices of building cluster "A."

KONG ET AL. 9 of 23

.com/doi/10.1029/2025JD044574 by Peking University Health, Wiley Online Library on [25/09/2025]. See the Terms and Conditions

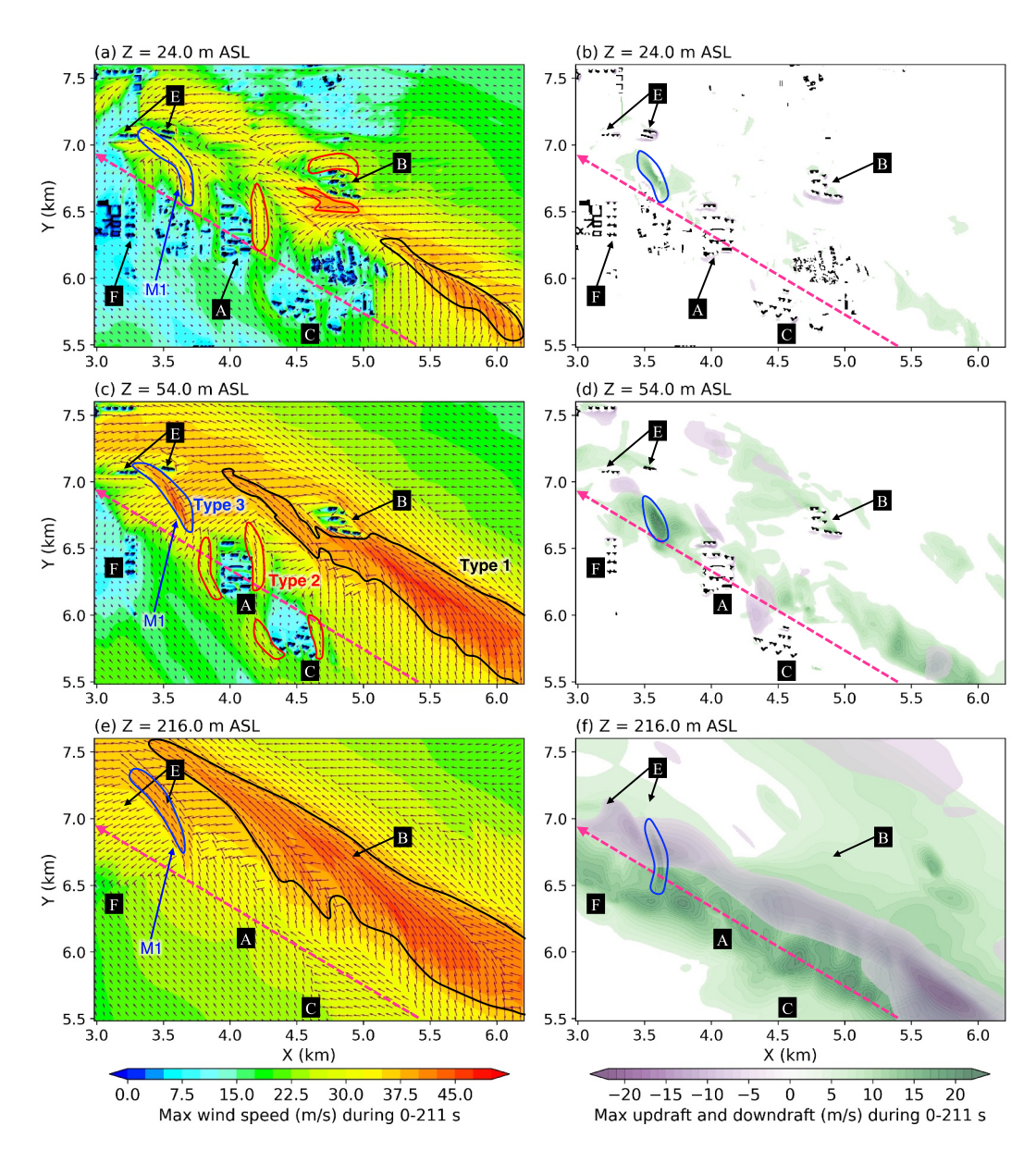


Figure 4. Patterns of maximum horizontal wind speeds (left column) and maximum vertical velocities (right column) in the analysis area (marked with white rectangle in Figure 2d) of different heights during the whole CTL run. (a–b) Z = 24.0 m above sea level (ASL). (c–d) Z = 54.0 m ASL. (e–f) Z = 216.0 m ASL. The absolute value threshold of vertical velocities to be plotted is 5 m s⁻¹. In the left column subplots, the purple vector at each given grid represents the wind direction at the moment when wind speed reaches its maximum. The magenta dashed line with an arrow in each subplot indicates the approximate tornado-like vortex track. Buildings above the plotting plane are shown in black while different high-rise building clusters are marked with white capital letters inside black boxes. Black, red and blue curves are used to mark the local strong winds of Type 1, Type 2, and Type 3, respectively or their corresponding vertical motions.

the simulated TLV tends to exhibit larger in size than the real tornado and a significant distance between Type 1 and the vortex center.

Since Type 1 are originated from the weather system, their patterns would become more turbulent downstream as disturbed by buildings. Even on a larger scale, ambient flows show high sensitivity to the heights of buildings. As shown by Figures 5a, 5b, 5d and 5e, the max wind speeds in CTL are lower than those in $0.5H_BLD$ and NO_BLD in most areas at Z=24.0 and 54.0 m ASL, indicating that the primary effect of the existence of buildings or their heightening seems like a decrease in wind speeds downstream from the buildings. Such an effect

KONG ET AL. 10 of 23

21698996, 2025, 17, Downloaded from https://agupubs.onlinelibrary.wiley.com/doi/10.1029/2025JD044574 by Peking University Health, Wiley Online Library on [25/09/2025]. See the Terms and Condi

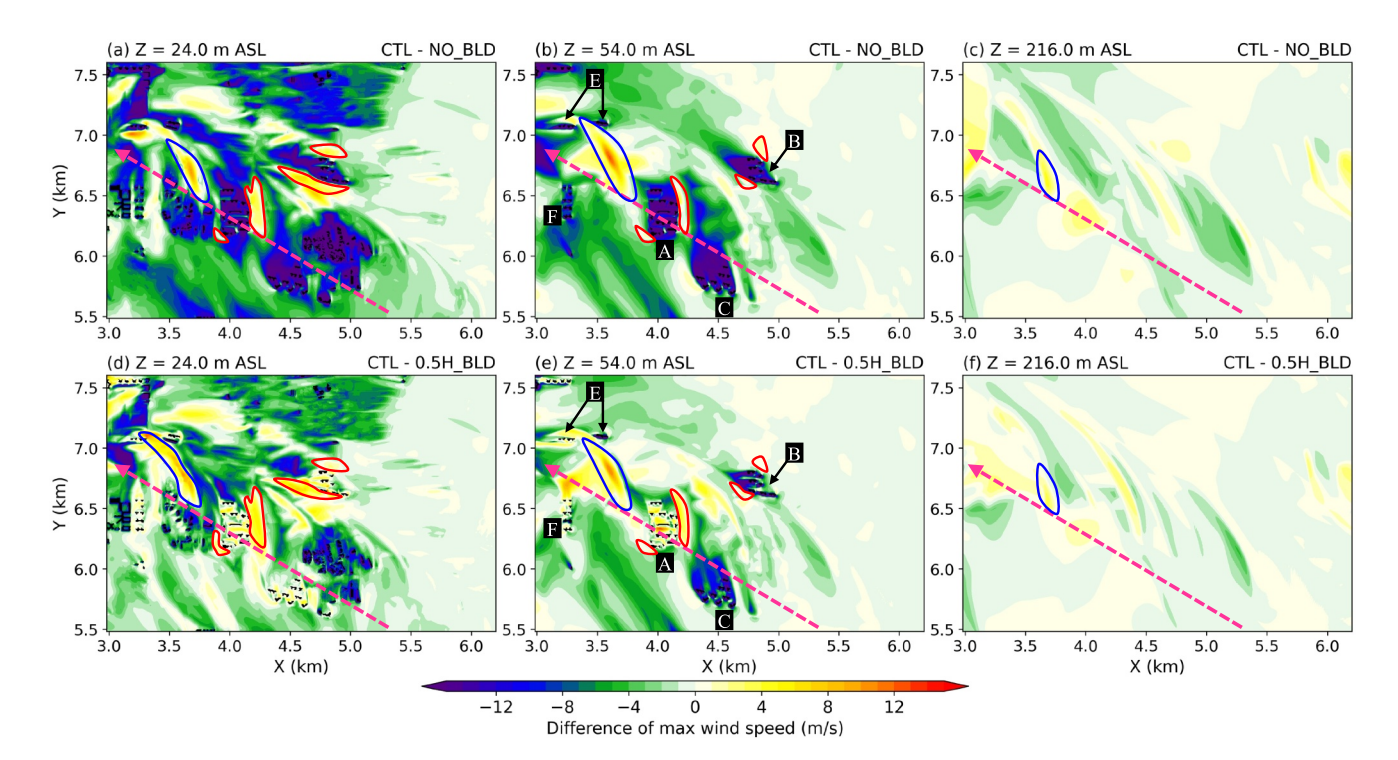


Figure 5. Difference of maximum wind speeds between CTL and sensitivity experiments about building heights. (a–c) Difference between CTL and 0.5H_BLD. (d–f) Difference between CTL and NO_BLD. (a and d) Z = 24.0 m above sea level (ASL). (b and e) Z = 54.0 m ASL. (c and f) Z = 216.0 m ASL. The magenta dashed line with arrow represents the approximate tornado-like vortex track. Buildings above the plotting plane are shown in black while different high-rise building clusters are marked with white capital letters inside black boxes. Blue curves indicate the locations of Type 3 local strong winds.

also works on Type 1. After being disturbed by building cluster "B," Type 1 are still seen in the downstream open area of "B," but with lower speeds (Figure 4c).

There are also small-scale local strong winds adjacent to high-rise buildings, which are classified as "Type 2" (Figure 4c). Type 2 local strong winds occur at the flanks of building clusters, such as those marked with red curves around "A" and "B." Figure 5b shows that in most downstream areas of building clusters in CTL, wind speeds are lower than NO_BLD. There are still lateral flanks of building clusters "A" and "B" showing around 0 or slightly larger than 0 (such as about $1-2 \text{ m s}^{-1}$ at the flanks of "B" at Z=54.0 m ASL) in the difference of maximum wind speeds between CTL and NO_BLD. Such relative acceleration is based on the high wind speeds of over 35 m s⁻¹ in NO_BLD, indicating that the winds are still hazardous in these building flanks. These strip-like flanks with acceleration compared to the surrounding neighborhood, extend for about 200–500 m, which are similar to the scales of the neighboring building clusters. Type 2 are also characterized by the wind direction slightly deviated by buildings. These features indicate that Type 2 are the flow acceleration locally induced by the blocking effects of buildings, which has been shown in other classic laboratory and numerical simulations of flow around bluff bodies (e.g., Hussein & Martinuzzi, 1996; Larousse et al., 1993; Oke et al., 2017).

Finally, in the open area among building clusters "A," "E" and "F," we focus on the local strong winds in the strip-like area marked with a blue curve in Figure 4c, which are classified as "Type 3." They extend from the northwest of building cluster "A" to the channel of building cluster "E." The occurrence of the Type 3 seems highly reliant on building clusters in this case. As shown by Figure 5, the max wind speeds in CTL where Type 3 occur are higher than the same area in $0.5H_BLD$ or NO_BLD even at Z=216.0 m ASL. It seems that the existence of buildings or their heightening leads to the formation or strengthening of Type 3. Different from Type 2 that are located at the flanks of buildings, Type 3 occur around the TLV but are closer to the core of TLV compared with Type 1. The wind direction of Type 3 turns from southerlies or southwesterlies to southeasterlies, which looks like the northeast quadrant of TLV's strong winds and it is similar to Type 1. These characteristics suggest that Type 3 might be the confined re-intensification of TLV cyclonic winds, when the TLV reorganize its structures after being disturbed by upstream building clusters.

KONG ET AL.

Besides the effects from the reorganization of TLV structures (discussed in detail in Section 4.2), the formation of Type 3 local strong winds is also related to the effects of "wind corridors." Here a wind corridor is defined as the neighborhood-scale (up to 1 or 2 km) band area of strong winds formed in the open areas among several building clusters along the direction of ambient flow. Specifically, these features should be identified by tracing back to the upstream sources of local strong winds along streamlines. Wind corridors are situated among building clusters in narrow shapes with speeds over 15 m s⁻¹, and exhibit higher wind speeds than the further upstream areas. As we have illustrated above, the experiments with higher buildings have stronger Type 3 (Figure 5). Such stronger Type 3 local strong winds are speculated to be led by the more well-defined wind corridors, which lead to more concentrated momentum transport. Wind corridors' generation is dominated by both the ambient flows by TLV and the configuration of building clusters. They are similar to the concepts of "urban ventilation corridors" in urban planning (e.g., Ren et al., 2018) and "gap winds" in mountain meteorology (e.g., Overland & Walter, 1981), since these concepts all feature a sort of fixed barriers on the underlying surface to channel the flows into a constricted passage. However, the involvement of the movable nature of small-scale TLV in our study causes rapid changes in these features, distinguishing them from the aforementioned concepts.

The wind corridors' evolution and their impacts on Type 3 local strong winds are examined through the snapshots of horizontal wind fields around key building clusters (Figure 6). At FCST = 131 s, the TLV main vortex is located in the open area among building clusters "A," "B" and "C" (Figure 6a). Convergent flows occur to both of its southwest (among "A," "C" and "D") and northeast (between "B" and "C"). However, since the strong wind quadrant of TLV is located to the east and north of the TLV main vortex, the wind corridor "C1" between "C" and "D" which points to the west of the main vortex is relatively weak. Meanwhile, we notice a building-lee vortex to the west of "A." At FCST = 143 s, as the TLV moves northwestward to the west of "A," "C1" is strengthened because it currently connects to the east strong wind quadrant of TLV along the channel between "A" and "C" (Figure 6b). To the east of "A," the original low-level TLV main vortex dissipates, while the vortex to the west of "A" becomes the most salient convergence zone around this area. Such phenomenon belongs to the reconstruction process of TLV structures when passing over "A," which will be further discussed in Section 4.2.

At FCST = 170 s, the TLV has moved away from building cluster "A" (Figure 6c). The wind corridor "C1" which connects to the east strong wind quadrant of TLV extends northwestwards. Due to the blocking effect of "A," "C1" is divided into two sub wind corridors "C1-1" (between "A" and "C") and "C1-2" (between "A" and the TLV). "C1-1" strengthens the flow to the east and northeast sides of "A." However, as the wake of "C" gradually turns to extend northwestward from northward during tens of seconds (cf., Figures 6b and 6c), the width of "C1-1" is being squeezed. On the other side of "A," "C1-2" starts to support the formation of local strong wind "M1." Now, the wind speed of "M1" is just over 20 m s⁻¹.

Then, at FCST = 197 s, as TLV continues moving northwestward, the more squeezed "C1-1" needs to detour a longer distance for the connection to the strong wind quadrant of TLV, and the wind speeds along this corridor decrease (Figure 6d). In contrast, the departure of TLV from "A" now makes "C1-2" become the main wind corridor, which has broadened the width of about one width scale of "A." Meanwhile, "M1" rapidly intensifies to the maximum wind speed (43.759 m s⁻¹) since the TLV started passing over buildings. The projection of shifting local speed maximum of "M1" on maximum field corresponds to the event of Type 3 marked with a blue curve in Figure 4c. In short, with the motion of TLV, wind corridors are established, strengthened and weakened subsequently in the open areas between high-rise building clusters. The broad main wind corridors provide an external surge of momentum to the generation of Type 3 local strong winds among buildings. Another local contributing factor to Type 3, the re-intensification of TLV, would be discussed in Section 4.2.

Characteristics of different types of local strong winds at lower and higher levels are also examined. At Z = 24.0 m ASL, wind speeds are generally lower than that at Z = 54.0 m ASL (cf., Figures 4a and 4c; see also Figure S3a in Supporting Information S1). This is not only because denser buildings produce more blocking on winds, but also due to the non-slip bottom boundary setting of our CFD model leading to smaller near-surface wind speeds. Among three types of local strong winds, the decrease in wind speed magnitude of Type 2 is not as much as Type 1 and Type 3 (Figure S3a in Supporting Information S1). The pattern of Type 2 around building cluster "B" is even more pronounced at Z = 24.0 m ASL than at higher levels (cf., Figures 4a and 4c; see also Figures 5a and 5b). Such features raise the relative importance of Type 2 near the ground level.

At Z = 216.0 m ASL where the influence of buildings is small, continuous Type 1 strong winds are seen from the southeast to the northwest of the plotting area (Figure 4e). Accompanying updrafts and downdrafts of the TLV are

KONG ET AL. 12 of 23

21698996, 2025, 17, Downloaded from https://agupubs.onlinelibrary.wiley.com/doi/10.1029/2025JD044574 by Peking University Health, Wiley Online Library on [25/09/2025]. See the Terms and Conditions (https://onlinelibrary.

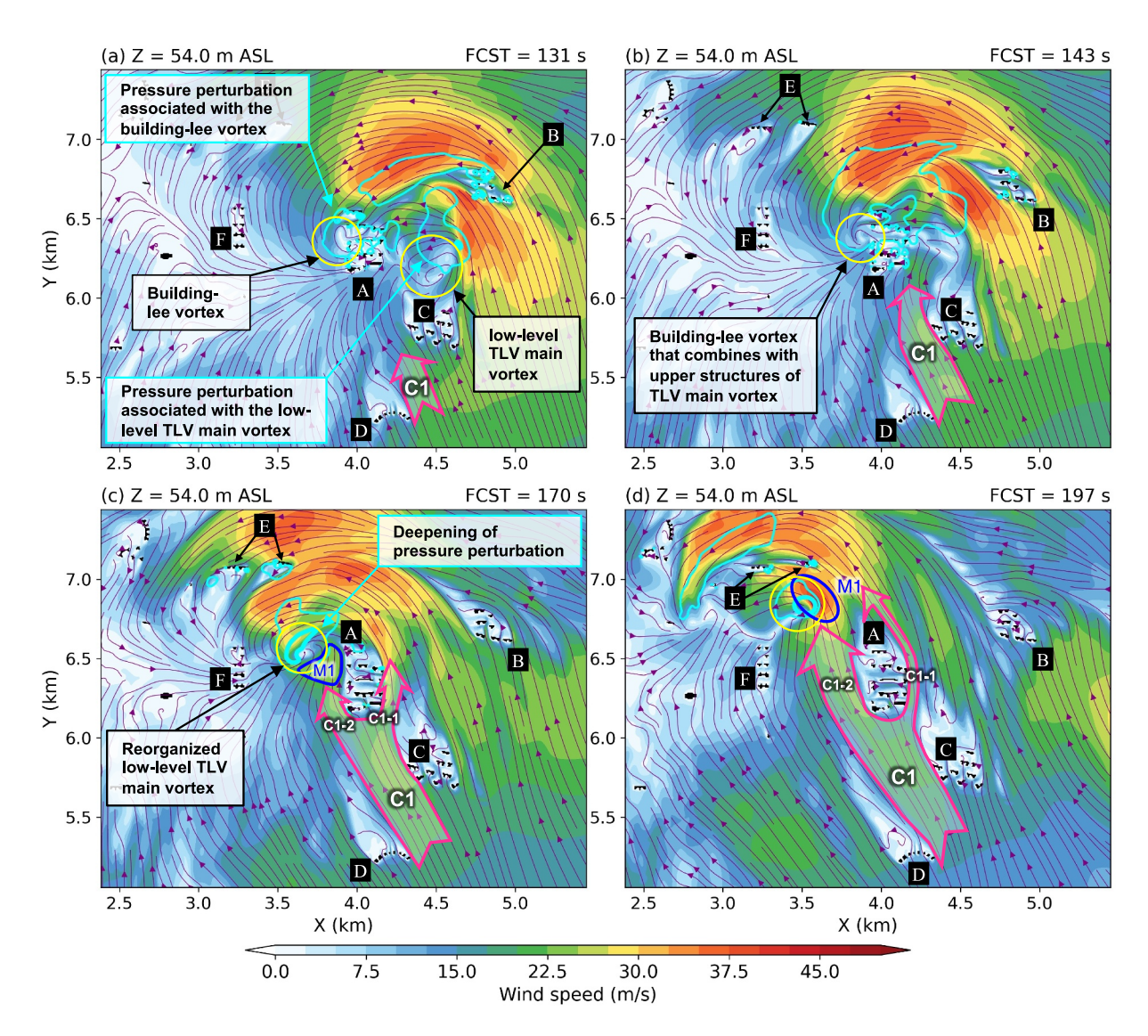


Figure 6. Same as Figure 3, but zoom in to focus on the key building clusters related to the evolution of wind corridors and local strong winds. Blue curves with lower-case letters are used to mark the instantaneous maximum speed cores of Type 3 local strong winds. Translucent magenta curve arrows indicate the locations of wind corridors. Yellow circles mark the vortices during the reconstruction of tornado-like vortex structures. Thin and thick cyan contour lines indicate P = 1,001 hPa and P = 999.5 hPa, respectively.

shown in adjacent areas (Figure 4f). Note that a real tornado may have updrafts greater than 75 m s⁻¹ just above the shallow inflow layer (Markowski & Richardson, 2010). Compared with the reality, the vertical motions produced by our WRF model with a coarse grid spacing are weak, but are still somewhat physically reasonable. Regarding an idealized vortex, if a maximum wind speed is given, a larger radius of maximum wind speed would correspond to weaker vortex-driven convergence. According to the continuity principle, the vertical motion driven by convergence would also be weaker. Even so, during the integration of our CFD model with a grid spacing of 6 m, the original weak vertical motions have become stronger before the TLV is disturbed by buildings (cf., Figures S5b and S5d in Supporting Information S1).

At Z = 216.0 m ASL, the strongest downdrafts are located along the southwest flank of the strip-like area of Type 1, a high gradient zone of horizontal wind speeds (cf., Figures 4e and 4f), suggesting the role of downdrafts in supporting Type 1 through intense downward momentum transport. Such downdrafts seem displaced from the center of our simulated TLV. On the one hand, it is because of our relatively coarse resolution of WRF. On the other hand, our CFD model nests the outputs from WRF only below 3126.9 m, which may gradually detach TLV structures from the influence of the parent supercell.

KONG ET AL. 13 of 23

For Type 1 in the upstream area of "B" at Z = 216.0 m ASL, their wind speeds are comparable to that at Z = 54.0 m ASL (both with maximum speeds of near 46 m s⁻¹). It indicates that Type 1 can generally maintain their intensity at such a relatively high level. At Z = 216.0 m ASL, Type 2 local strong winds along the flanks of buildings cannot be found. In contrast, Type 3 local strong winds can still be seen among building clusters "A," "E" and "F," indicating that the effects of wind corridors can extend over buildings. Type 3 in each layer are accompanied with local strong updrafts (marked with blue curves in Figures 4b, 4d and 4f), which are speculated to be caused by the horizontal convergence of the reorganized TLV structures after passing over "A" (Figure 6d).

4.2. Reconstruction of TLV Structures Passing Over High-Rise Building Clusters

Here, we examine the detailed variations of TLV structures that pass over high-rise building clusters using modeling results and video records. In Figure 7, the left column shows the main flow patterns of TLV by the streamlines originating from the near-surface layer. The middle column of Figure 7 shows the fine-scale features of TLV by isosurfaces of vertical vorticity. Note that, the TLV moves from the top left to the bottom right in these figures, and passes over the building cluster "A" in the center. The right column of Figure 7 shows the screenshots of different phases of tornadic CF obtained from the video taken by a local resident. As shown by a damage map derived from damage surveys (Figure 3 in Bai et al. (2017)), the analyzed tornado centerline passes through the video-caught building cluster "Boaocheng" (BAC), so the evolution of CF in the video can be regarded as the result of building effects of BAC. BAC has 14 buildings near 75–100 m, which is comparable to the height of "A" in the CFD model.

At FCST = 115 s, the TLV is approaching building cluster "A." The main vortex of TLV is characterized by the slantwise upward streamlines spiraling around the TLV's center, as shown in the upper left of Figure 7a. In detail, the fine-scale structures of the TLV are featured by several local columns of high vertical vorticity arranged in a ring-like pattern around the TLV's center in the upper left of Figure 7b. Such structures are the so-called ring-vortex, which are commonly seen in high-resolution mesoscale simulations of tornadoes (e.g., J. Li et al., 2022; Zhu & Zhao, 2022). In the middle right of Figure 7b, downwind from building cluster "A," a local column of large vertical vorticity at a smaller scale than "A" is established ahead of the TLV main vortex, which corresponds to the building-lee vortex to the west of "A" in Figures 3e, 3f and 6a. The well-defined structures of the simulated TLV correspond well to the observed relatively intact condensation funnel "CF1" in the screenshots of Figures 7c and 7d before passing BAC.

At FCST = 131 s, the TLV main vortex is strongly disturbed by building cluster "A." The disturbance on the TLV appears most pronounced below about twice the height of building cluster "A," where the low-level part of TLV main vortex is blocked by "A" (Figure 7e). In contrast, the upper part of the TLV main vortex is still well defined and continues moving downstream above "A." In Figure 7f, the building-lee vortex intensifies in the downstream of "A." It is stretched from about one height of "A" to 1.3 times the height of "A," which may be induced by the updrafts of TLV (refer to Figure 7a). This vortex and the TLV main vortex are each accompanied by distinct low-level pressure perturbations (Figure 6a). The building-induced local low pressure may attract tornado main vortex moving toward it (Kawaguchi et al., 2019). The screenshots of Figures 7g and 7h show that the observed "CF1" becomes scattered above BAC, corresponding to the disturbed main vortex of the simulated TLV. Meanwhile, a newly formed "CF2" is observed above the downstream of BAC, which is similar to the strengthening building-lee vortex in the model.

At FCST = 143 s, the upper part of TLV main vortex moves above the local building-lee vortex and combines with each other, while the original low-level part of TLV main vortex gradually dissipates (Figure 7i). Figure 7j further shows that the column of the building-lee vortex grows taller and thicker and develops to the strongest vortex column in the ring-vortex. More importantly, the column of building-lee vortex detaches building cluster "A" from now on with the motion of the ring-vortex, indicating that the building-lee vortex is merged with the TLV. From a perspective of the horizontal plane, it looks like that the building-lee vortex in the downstream of "A" "replaces" the original low-level TLV main vortex in the upstream (cf., Figures 6b and 6a). From a 3-D perspective, TLV structures are being reconstructed with their interaction with the building-lee vortex when passing over "A." Likewise, in video records shown in Figures 7k and 7l, "CF1" is dissipating above BAC, while "CF2" gradually touches down in the downstream. The observed "CF2" corresponds well to the strongest vortex column in the CFD model when the TLV main vortex combines with the building-lee vortex. In the 0.5H_BLD

KONG ET AL. 14 of 23

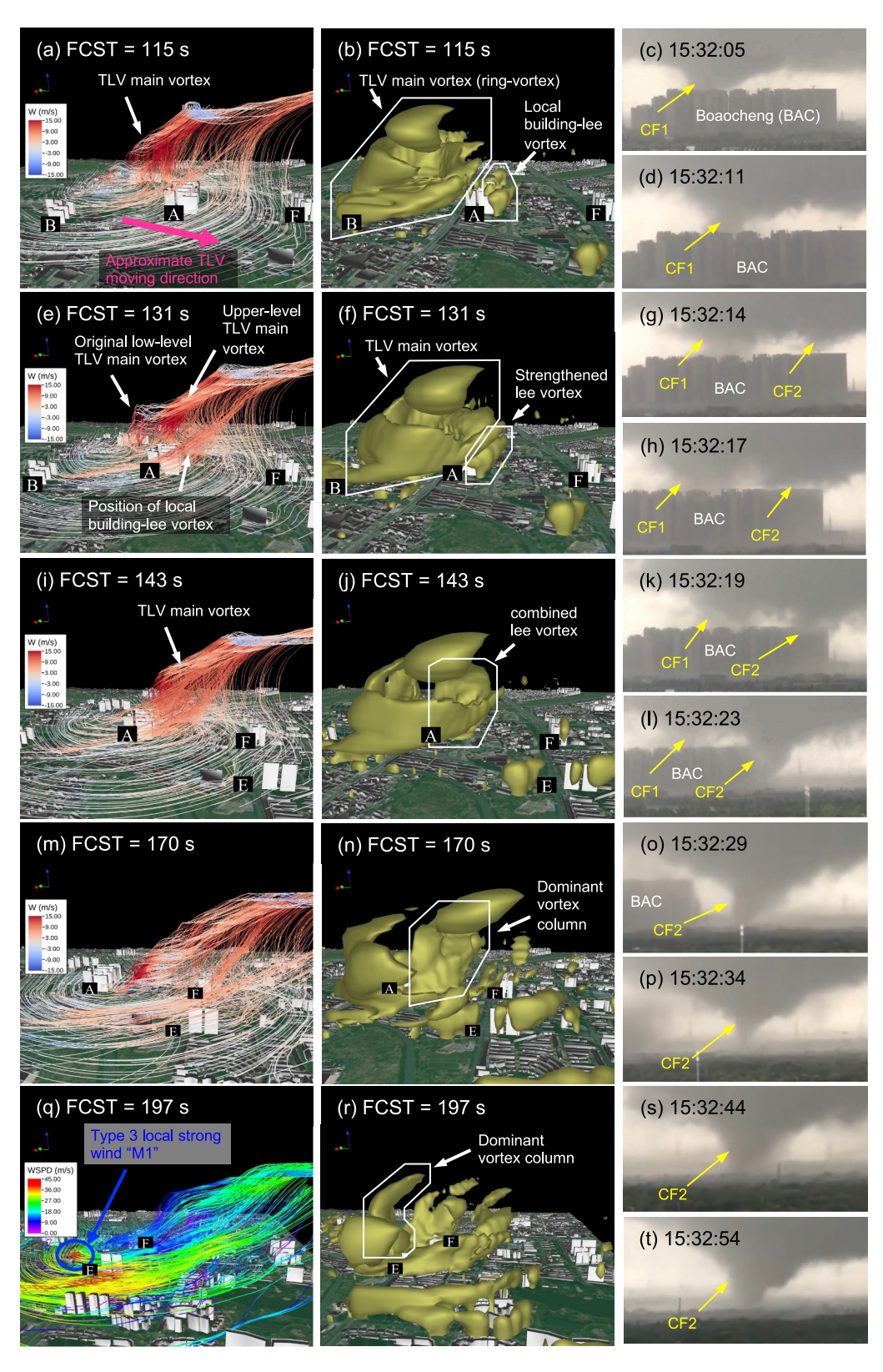


Figure 7.

KONG ET AL. 15 of 23

experiment where the heights of all buildings are halved, the reconstruction of TLV structures can still be seen like that in CTL, while the observable height of the reconstruction decreases (not shown in figures).

At FCST = 170 s, the TLV has moved half the width scale of "A" away from "A," so that no obvious vortices appear immediately downwind from "A" (Figure 7m). The vortex column which is merged by the local building-lee vortex becomes more dominant in the ring-vortex (Figure 7n), accompanied with the deepening of pressure perturbation (Figure 6c). However, other vortex columns which surround the dominant one decay, indicating that the overall intensity of the TLV becomes weaker than that at the former timestep (cf., Figures 7j and 7n). Also, the maximum wind speed around the TLV at Z = 54 m ASL decreases from 39.545 m s⁻¹ at FCST = 143 s to 37.037 m s⁻¹ at 170 s. The weakening of the TLV is attributed to the strong disturbance by "A" tens of seconds before. In the video, the scale of "CF2" is shrinking after moving away from BAC (Figures 7o and 7p), suggesting that the spatial range of strong winds of the real tornado may become narrow. Such observed shrinking of "CF2" corresponds to the weakening of the simulated TLV.

At FCST = 197 s, the TLV re-intensifies in the downstream open area of building cluster "A," about one width scale of "A" away from "A." Now the TLV is characterized by the thicker and higher vortex columns of the ring-vortex than those at FCST = 170 s (cf., Figures 7r and 7n). Such recovery of intensity is also shown in near-surface wind speeds. Figure 6d shows that the speed of Type 3 local strong winds in the zone labeled "M1" reaches their maximum (43.759 m s⁻¹) near TLV's center, with much higher wind speeds than at 170 s (37.037 m s⁻¹). The location of this wind speed maximum coincides with the dominant vortex column in Figure 7r.

The maximum wind speed in the zone of "M1" at FCST = 197 s is $43.759 \,\mathrm{m\,s^{-1}}$. The intensification of "M1" to such a high speed of near $44 \,\mathrm{m\,s^{-1}}$ can be attributed to two contributing factors. As we have discussed in Section 4.1, one contributing factor is that the main wind corridor "C1-2" provides an external surge of momentum for "M1." The contribution of the wind corridor to "M1" is approximately 25 m s⁻¹, which can be inferred from the wind speeds at the slight upstream of "M1" (Figure 6d). Meanwhile, the enough space favors the re-intensification of the TLV, which further increases the wind speeds of "M1" near the center of the TLV and thus is regarded as another local contributing factor to the wind speeds in "M1." According to the above rough analysis of the contribution to "M1," the re-intensification of the TLV is likely to contribute about 19 m s⁻¹. Therefore, the wind corridor may play a primary role in the generation of Type 3 local strong wind "M1" in this case.

Likewise, the video records show the widening of "CF2" (Figures 7s and 7t), which may suggest the recovery of the spatial range of strong winds after the reorganization of tornado structures. Moreover, the damage map (Figure 3 in Bai et al. (2017)) shows that the tornado's damage intensity didn't recover obvious range of EF1 until the tornado detached BAC for approximately one length scale of BAC, though there is uncertainty in the damage survey results. Such evolutionary characteristics of damage are also similar to the evolutionary characteristics of the intensity of our simulated TLV.

5. Sensitivity of TLV Structures and Local Winds to Buildings' Configurations

First, the sensitivity of the evolution of TLV structures to the slight shift of building clusters is investigated. In CTL, the TLV passes over the middle of building cluster "A," and then its low-level structures are reconstructed characterized by the vertical alignment of the original aloft TLV part and building-induced lee vortex near ground (Figure 8d). In our two additional sensitivity experiments (hereafter referred as BLD_N and BLD_S, respectively), the topography including buildings is artificially moved farther north or south for 250 m (near one horizontal width of building clusters), so that the impacts of that TLV passes different sides of building clusters can be investigated.

Figure 7. Evolution of the simulated tornado-like vortex (TLV) or observed tornado structures. (a), (b), (e), (f), (i), (j), (m), (n), (q) and (r) are the instantaneous modeling results. Streamlines are shown in (a), (e), (i), (m) and (q) and their shading represents vertical velocities, except the shading in (q) represents horizontal wind speeds. The isosurfaces in (b), (f), (j), (n) and (r) represents vertical vorticity of $0.125 \, \text{s}^{-1}$. The left and middle subfigures in the same row share the same camera viewpoint, while the camera across different rows only changes its position along the moving TLV without changing its orientation. The capital letters with black boxes mark building clusters. (c), (d), (g), (h), (k), (l), (o), (p), (s) and (t) are the screenshots from a real video taken on 4 October 2015 during the Foshan tornado event, which shows the tornado and its condensation funnel (CF, marked with yellow arrows) passing over a building cluster.

KONG ET AL. 16 of 23

from https://agupubs.onlinelibrary.wiley.com/doi/10.1029/2025JD044574 by Peking University Health, Wiley Online Library on [25/09/2025]. See the Terms and Conditions (https://agupubs.onlinelibrary.wiley.com/doi/10.1029/2025JD044574 by Peking University Health, Wiley Online Library on [25/09/2025]. See the Terms and Conditions (https://agupubs.onlinelibrary.wiley.com/doi/10.1029/2025JD044574 by Peking University Health, Wiley Online Library on [25/09/2025]. See the Terms and Conditions (https://agupubs.onlinelibrary.wiley.com/doi/10.1029/2025JD044574 by Peking University Health, Wiley Online Library on [25/09/2025]. See the Terms and Conditions (https://agupubs.onlinelibrary.wiley.com/doi/10.1029/2025JD044574 by Peking University Health, Wiley Online Library on [25/09/2025]. See the Terms and Conditions (https://agupubs.onlinelibrary.wiley.com/doi/10.1029/2025JD044574 by Peking University Health, Wiley Online Library on [25/09/2025].

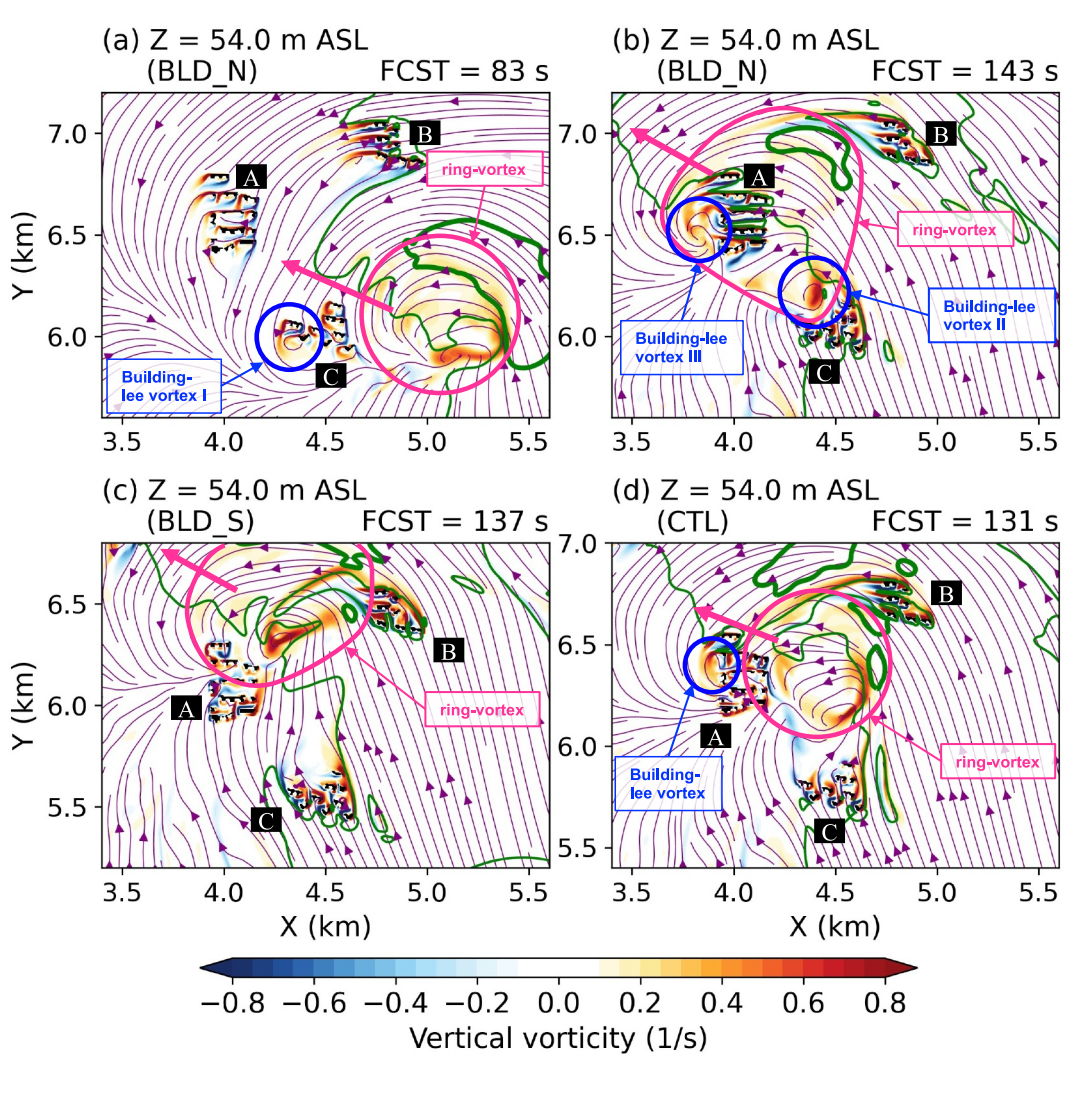


Figure 8. Instantaneous vertical vorticity (shading) and the direction of winds (streamlines) at Z = 54.0 m above sea level when tornado-like vortex (TLV) passes building cluster "A," "B," and "C" in different sensitivity experiments. (a) and (b) FCST = 83 and 143 s in BLD_N, respectively. (c) FCST = 137 s in BLD_S. (d) FCST = 131 s in CTL. Thin and thick green contour lines indicate horizontal wind speed V = 20 m s⁻¹ and V = 35 m s⁻¹, respectively. The magenta arrows indicate the approximate TLV moving directions. The magenta and blue circles mark the approximate locations of the ringvortex and local building-lee vortices, respectively. Buildings above the plotting plane are shown in black.

In BLD_S (Figure 8c), the TLV structures generally keep stable and no reconstructions occur around any building clusters, since the TLV passes through the open area between building clusters without obstructions. However, the vertical vorticity generated downwind from "B" may contribute to the ring-vortex structure of TLV.

In BLD_N, the obstruction of building clusters in TLV's moving direction makes the reconstruction of TLV structures possible. The building-lee vortices contribute differentially to the vertical vorticity of TLV's ring-vortex, while whether they vertically align with the aloft TLV structures decides whether they can merge with TLV and move downstream. Before the TLV passes building cluster "C," building-lee vortex "I" is formed to the south of "C" (Figure 8a). Afterward, the upper TLV structures pass over the north of "A," resulting in the displacement of the aloft TLV structures and building-lee vortex "I." However, as stretched by the TLV's updrafts, the vertical vorticity from this building-lee vortex can temporarily contribute to the ring-vortex. As the TLV moves northwestwards, southerlies gradually increase to the south of "C," leading to the dissipation of building-lee vortex "I" (Figure 8b). To the north of "C," background southerlies favor another building-lee vortex "II," and such a lee vortex vertically corresponds better with the TLV structures aloft. Therefore, the building-lee vortex "II" is rapidly merged to the ring-vortex and moves downstream.

KONG ET AL. 17 of 23

21698996, 2025, 17, Downloaded from https://agupubs.onlinelibrary.wiley.com/doi/10.1029/2025JD044574 by Peking University Health, Wiley Online Library on [25/09/2025]. See the Terms and Conditions (https://onlinelibrary.

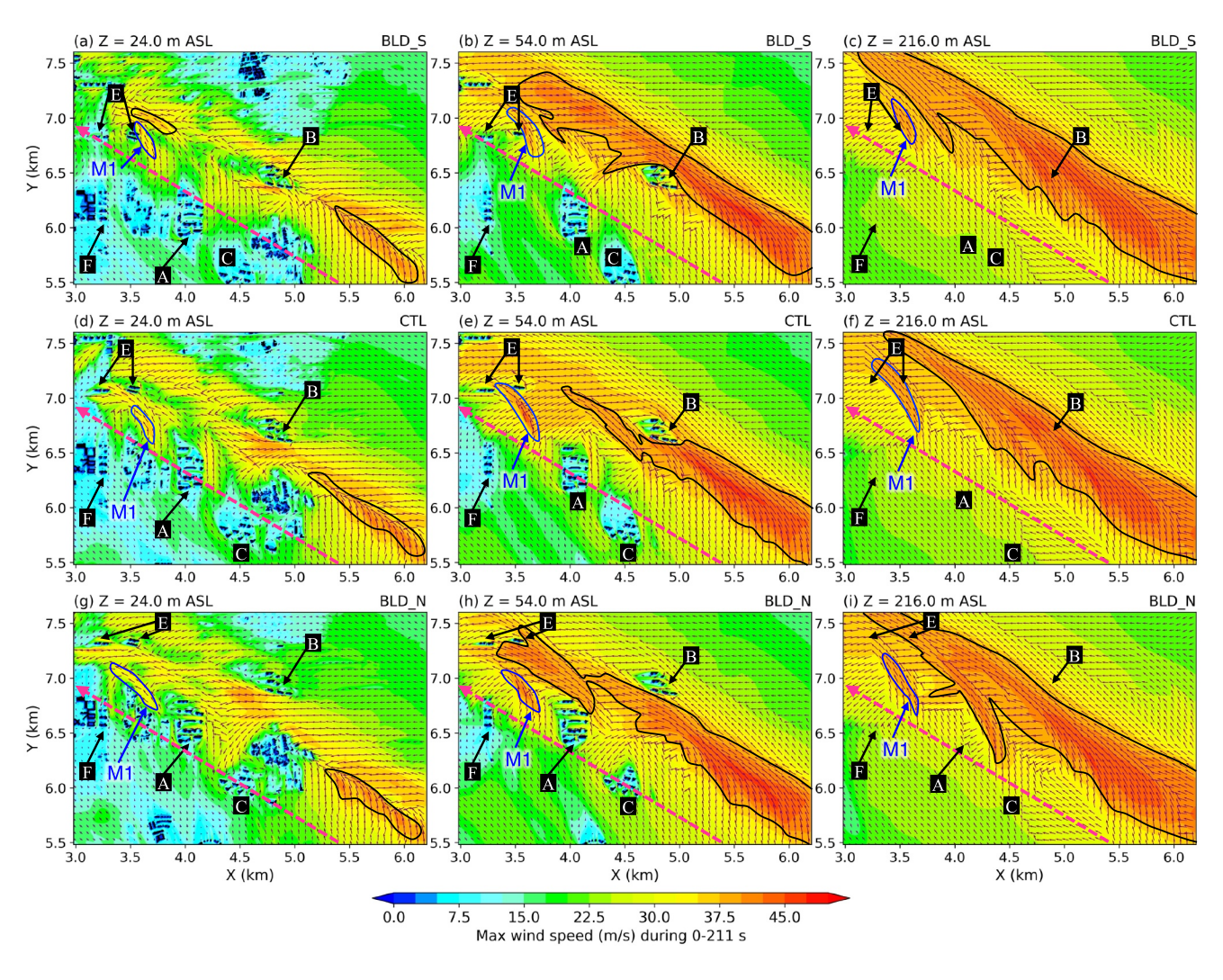


Figure 9. Patterns of maximum horizontal wind speeds in CTL and sensitivity experiments about buildings' configurations. (a)—(c) BLD_S. (d)—(f) CTL. (g)—(i) BLD_N. (a, d and g) Z = 24.0 m above sea level (ASL). (b, e and h) Z = 54.0 m ASL. (c, f and i) Z = 216.0 m ASL. The purple vector at each given grid represents the wind direction at the moment when wind speed reaches its maximum. The magenta dashed line with arrow in each subplot indicates the approximate tornado-like vortex track. Buildings above the plotting plane are shown in black while different high-rise building clusters are marked with white capital letters inside black boxes. Black and blue curves are used to mark the local strong winds of Type 1 and Type 3, respectively.

When the TLV just passes building cluster "C," building-lee vortex "III" can also be seen to the west of "A," which is located in the direction that the upper structures of TLV pass (Figure 8b). Subsequently, this building-lee vortex is merged to the ring-vortex of TLV and moves downstream. Such a scene is similar to that observed in CTL around "A," though the building-lee vortex in BLD_N is located slightly further south. Interestingly, both building-lee vortices "III" and "II" detach their affiliated building clusters and move downstream around the same timestep (Movie S1). This phenomenon may be a result of the two lee vortices belonging to the same ring-vortex currently, so that they are simultaneously guided by upper TLV structures. From a visual perspective, this phenomenon may suggest that the tornadic CF could be formed and move concurrently both in the upstream and downstream of "A," or it could be directly re-established to the west of "A" after dissipation to the east of "C."

Next, we investigate the sensitivity of TLV-associated local strong winds to the configurations of buildings by examining the maximum winds in BLD_S, CTL and BLD_N (Figure 9). For Type 1 local strong winds at Z = 216.0 m ASL, their patterns are similar among three experiments except some details (Figures 9c, 9f, and 9i; see also Figures S4c and S4f in Supporting Information S1). At Z = 54.0 m ASL, the patterns of Type 1 in the

KONG ET AL. 18 of 23

upstream of building cluster "B" are also generally consistent among three experiments (Figures 9b, 9e, and 9h; see also Figures S4b and S4e in Supporting Information S1), while differences are shown in the downstream of "B." In CTL, the maximum wind speed downstream of "B" is obviously smaller than those in BLD_S and BLD_N. Such weaker winds may result from the blocking of "B" exactly in the middle of the swath of Type 1, which induces strong disturbances on wind speeds. Therefore, Type 1 may be sensitive to the existence of building clusters along their impact swath.

For Type 3 local strong winds, we focus on "M1" located among building clusters "A," "E" and "F" in CTL (Figures 9d–9f, $X \sim 3.6$ km, $Y \sim 6.6$ km). Note that in BLD_S (Figures 9a–9c; see also Figures S4a and S4c in Supporting Information S1) and BLD_N (Figures 9g–9i; see also Figures S4d and S4f in Supporting Information S1), "M1" have almost the same occurrence positions as that in CTL, which seems that they are insensitive to the slight change in configurations of buildings. Vertically, "M1" in BLD_S and BLD_N can also extend from Z = 24.0–216.0 m ASL as those in CTL. In Section 4.1, we obtain that Type 3 are associated with the wind corridors generated by building clusters and TLV inflow. In BLD_S and BLD_N, the wind corridors in the upstream of "M1" (especially for "C1-2") have similar configurations to that in CTL, since the relative locations of the TLV track and building clusters are only changed less than one width of the strong wind quadrant of the TLV (cf., Figure 6; Figures S1 and S2 in Supporting Information S1). This may explain why such "M1" occur at almost the same locations in all three experiments. Therefore, Type 3 seem not so sensitive to the slight change of buildings' configurations or tornado's tracks, as the configurations of related wind corridors keep generally unchanged. The sensitivity tests of these two types of local strong winds provide insight into possible wind speed changes when tornadoes encounter buildings.

6. Summary

This study investigates a strong tornado intruding an urban area with high-rise buildings by employing a mesoscale-to-LES modeling system at a finest grid spacing of 6 m. A simulated TLV is obtained, and its characteristics show partial agreement to that of the real tornado, as shown by the qualitative comparisons of radar observations, video evidence and damage surveys. We examine the evolution of TLV structures and the characteristics and formation of associated local strong winds under the interaction of TLV and building-induced disturbances. The key findings are summarized below and in the schematic diagram of Figure 10.

The TLV is disturbed and reconstructed when passing over building clusters, and such a process can be divided into three main stages. In the first stage (disturbance stage), a local building-lee vortex, the key disturbance, is generated and stretched upwards, as the TLV with still largely undisturbed structures approaches the building cluster (Figures 10a and 10c). In the second stage (reorganization stage), the low-level part of the TLV main vortex has been blocked by the building cluster, leading to its weakening and gradual dissipation. Meanwhile, the upper part of the TLV keeps intact and continues moving above the building-lee vortex (Figure 10b). Then, the building-lee vortex becomes the new lower structure, and the original upper structures of the TLV undergo reorganization and gradually merge with the new lower one. Only the building-lee vortex that vertically aligns with the upper TLV structures can be merged with the TLV and continue to move downstream. In this stage, the TLV is temporarily weakened since the original TLV structures have been strongly disturbed. Finally, in the third stage, the TLV is re-intensified (re-intensification stage). The departure of TLV from the building cluster leaves enough space for the corridor of inflow, and also for the re-intensification of TLV (Figure 10d). Both the external surge of momentum provided by wind corridors among building clusters, and the re-intensification of TLV, favor the re-intensification of the local strong winds of the TLV.

Previous idealized experiments have provided some sketches of different stages of such a TLV reconstruction process. For example, Yang et al. (2011) showed that building-lee vortices can be generated in tornado-like winds, similar to our modeled building-lee vortices in the disturbance stage. Gorecki and Selvam (2013) demonstrated that when an idealized tornadic vortex passed over an idealized building, it split a vortex tip in the downstream of the building. Such a scene is similar to our reorganization stage, in which both the blocked original low-level part of the TLV and the building-lee vortex are connected to the upper part of the TLV at the same time. Kawaguchi et al. (2019) also showed that the strong vertical vortices at the corners of buildings are stretched upward and merged with the main structure of the tornado. In the simulation by Lewellen (2014), a tornado is weakened at first and re-intensified afterward when passing over blocks of buildings, corresponding to our modeled re-intensification of the TLV after leaving the building cluster. In our study, the whole reconstruction

KONG ET AL. 19 of 23



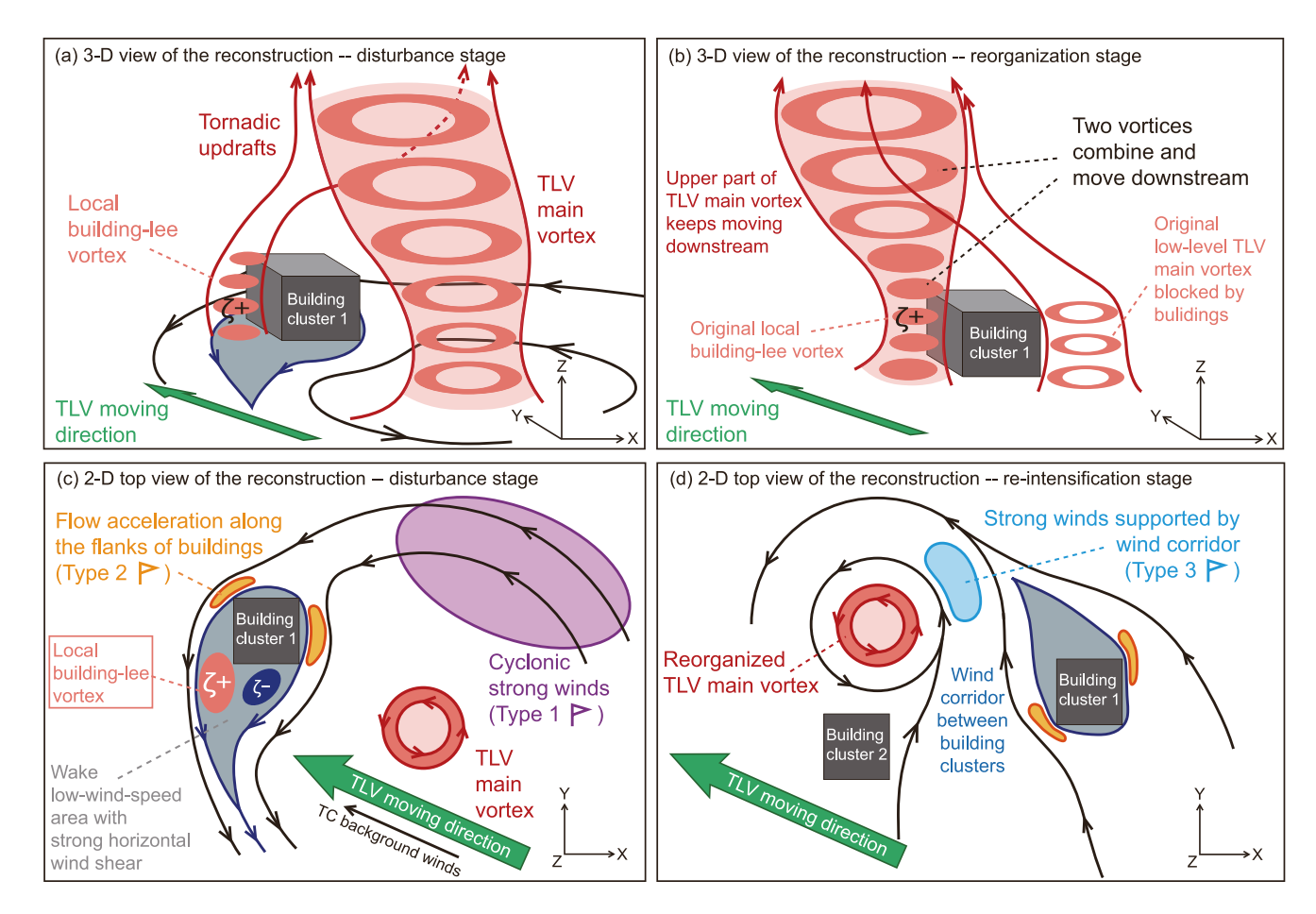


Figure 10. Schematic diagram of the reconstruction of tornado-like vortex (TLV) structures passing over high-rise building clusters and three types of TLV related local strong winds, depicted based on the results of this case modeling. (a)–(b) Three-dimensional view. (c)–(d) Two-dimensional top view. (a) and (c) Disturbance stage. (b) Reorganization stage. (d) Re-intensification stage.

process of the TLV is simulated under realistic weather conditions, and is linked to the observed tornadic CF which is disturbed and re-established when passing over a real high-rise building cluster.

The TLV-associated local strong winds in urban areas are classified into three types based on their different characteristics and causes, as shown in Figures 10c and 10d. Type 1 are the cyclonic ambient strong winds of TLV, with the largest scale and highest speed among all three types. They would be weakened by the blocking of buildings. Type 2 local strong winds are the flow acceleration along the flanks of building clusters under the TLV-induced background flow. Type 3 local strong winds can be regarded as the confined re-intensification of TLV cyclonic winds, resulting from both local increased rotation velocities from the re-intensifying TLV and external surge of momentum from wind corridors. Type 3 should be generated with the participation of building clusters, but can extend over buildings. Higher building clusters may enhance the acceleration of wind corridors and favor stronger Type 3. Given that the overall configurations of wind corridors remains unchanged, Type 3 can still occur at almost the same positions even if the locations of buildings change less than one width of the strong wind quadrant of the TLV. The introduction of these three types of local strong winds may be useful for qualitatively evaluating the complex strong winds in urban areas brought by tornadoes.

This study demonstrates the capability of assessing street-level strong winds in urban tornado events using our mesoscale-to-LES modeling system, and provides more knowledge of how the tornado evolves in urban areas. There are some aspects to be improved. First, it is necessary to upgrade the modeling system with more advanced configurations, such as the refinement in the resolution of mesoscale models. If the CFD model is integrated with the mesoscale modeling results that can directly resolve fine-scale tornado structures (e.g., Kawaguchi et al., 2019, 2020; J. Li et al., 2022), the reliability of our findings could be enhanced under more realistic

KONG ET AL. 20 of 23

21698996, 2025, 17, Downloaded

Acknowledgments
The authors are grateful to three

anonymous reviewers that help to improve

Southern Marine Science and Engineering

our manuscript. This study is funded by

(SML2024SP034), the National Natural

Science Foundation of China (42275002,

Meteorological Administration Tornado

the Science and Technology Research

Project of Guangdong Meteorological

Administration (GRMC2020013), The

authors thank the support from the Foshan

Tornado Research Center, and also thank

the National Supercomputing Center in

Guangzhou for providing the

supercomputing resource.

Key Open Laboratory (TKL202304), and

Guangdong Laboratory (Zhuhai)

42275006 and 42030604), China

conditions. Also, it is better to incorporate a turbulence injection method in the CFD model like that used in Bryan et al. (2017) and Kawaguchi et al. (2019, 2020), for a more realistic description of wind perturbations.

Second, when the TLV passes a building cluster, we hypothesize that the vertical vorticity generated by the local building-lee vortex may contribute to the reconstruction of the TLV at low levels. If the TLV slightly deviates its track so that it is not merged by the building-lee vortex, the impact on its subsequent intensity by the reduction of vertical vorticity contribution needs careful quantitative examination in the future.

Finally, the generalization of our preliminary findings from a limited number of sensitivity tests requires further investigation, such as how wind speeds change across a spectrum of different tornado intensities or sizes, and above a spectrum of urban areas with different morphology parameters.

Data Availability Statement

The CFD model is not accessible to the public because of the licensing policies and regulations under Sun Yat-sen University. It is available only upon request under a research agreement. The CFD modeling outputs, derived maximum wind fields in the analysis area, the topography including building data, the Python codes used to produce the figures, as well as the namelist of WRF simulation are available in the references (specifically Kong et al. (2025)). The software used to plot 3-D figures is VAPOR (S. Li et al., 2019; Visualization & Analysis Systems Technologies, 2023).

References

American Meteorological Society. (2012). Tornadic vortex signature. Glossary of Meteorology. Retrieved from http://glossary.ametsoc.org/wiki/ Tornadic_vortex_signature

Ashley, W. S., Strader, S., Rosencrants, T., & Krmenec, A. J. (2014). Spatiotemporal changes in tornado hazard exposure: The case of the expanding bull's-eye effect in Chicago, Illinois. *Weather, Climate, and Society, 6*(2), 175–193. https://doi.org/10.1175/WCAS-D-13-00047.1 Badmus, A. A., & Sutley, E. J. (2025). State-of-the-art review on reducing residential buildings' risk to tornado hazards. *Frontiers in Built Environment, 11*, 1543800. https://doi.org/10.3389/fbuil.2025.1543800

Bai, L., Meng, Z., Huang, L., Yan, L., Li, Z., Mai, X., et al. (2017). An integrated damage, visual, and radar analysis of the 2015 Foshan, Guangdong, EF3 tornado in China produced by the landfalling Typhoon Mujigae (2015). Bulletin of the American Meteorological Society, 98(12), 2619–2640. https://doi.org/10.1175/BAMS-D-16-0015.1

Beck, V., & Dotzek, N. (2010). Reconstruction of near-surface tornado wind fields from forest damage. *Journal of Applied Meteorology and Climatology*, 49(7), 1517–1537. https://doi.org/10.1175/2010JAMC2254.1

Bornstein, R. D., & Thompson, W. T. (1981). Effects of frictionally retarded sea breeze and synoptic frontal passages on sulfur dioxide concentrations in New York City. *Journal of Applied Meteorology and Climatology*, 20(8), 843–858. https://doi.org/10.1175/1520-0450(1981) 020<0843:EOFRSB>2.0.CO:2

Bryan, G. H., Dahl, N. A., Nolan, D. S., & Rotunno, R. (2017). An eddy injection method for large-eddy simulations of tornado-like vortices. Monthly Weather Review, 145(5), 1937–1961. https://doi.org/10.1175/MWR-D-16-0339.1

Chen, G., Iwai, H., Ishii, S., Saito, K., Seko, H., Sha, W., & Iwasaki, T. (2019). Structures of the sea-breeze front in dual-Doppler lidar observation and coupled mesoscale-to-LES modeling. *Journal of Geophysical Research: Atmospheres*, 124(5), 2397–2413. https://doi.org/10.1029/2018JD029017

Chen, G., Zhu, X., Sha, W., Iwasaki, T., Seko, H., Saito, K., et al. (2015). Toward improved forecasts of sea-breeze horizontal convective rolls at super high resolutions. Part I: Configuration and verification of a Down-Scaling Simulation System (DS3). *Monthly Weather Review*, 143(5), 1849–1872. https://doi.org/10.1175/MWR-D-14-00212.1

Cusack, S. (2014). Increased tornado hazard in large metropolitan areas. Atmospheric Research, 149, 255–262. https://doi.org/10.1016/j.atmosres. 2014.06.015

Du, S., Zhang, X., Jin, X., Zhou, X., & Shi, X. (2022). A review of multi-scale modelling, assessment, and improvement methods of the urban thermal and wind environment. *Building and Environment*, 213, 108860. https://doi.org/10.1016/j.buildenv.2022.108860

Dunn, L. B., & Vasiloff, S. V. (2001). Tornadogenesis and operational considerations of the 11 August 1999 Salt Lake City tornado as seen from two different Doppler radars. Weather and Forecasting, 16(4), 377–398. https://doi.org/10.1175/1520-0434(2001)016<0377:TAOCOT>2.0. CO;2

Edwards, R., & Schaefer, J. (2025). Downtown tornadoes. Storm Prediction Center. Retrieved from https://www.spc.noaa.gov/faq/tornado/downtown.html

Fiedler, B. H. (1998). Wind-speed limits in numerically simulated tornadoes with suction vortices. *Quarterly Journal of the Royal Meteorological Society*, 124(551), 2377–2392. https://doi.org/10.1002/qj.49712455110

Fujita, T. T., Watanabe, K., Tsuchiya, K., & Shimada, M. (1972). Typhoon-associated tornadoes in Japan and new evidence of suction vortices in a tornado near Tokyo (1). *Journal of the Meteorological Society of Japan*, 50(5), 431–453. https://doi.org/10.2151/jmsj1965.50.5_431

Gorecki, P., & Selvam, R. P. (2013). Three-dimensional simulation of tornado over complex terrain. In Paper Presented at 12th Americas Conference on Wind Engineering (12ACWE), Seattle, Washington, USA.

Huang, Z., Fan, X., Cai, L., & Shi, S. Q. (2016). Tornado hazard for structural engineering. Natural Hazards, 83, 1821–1842. https://doi.org/10.1007/s11069-016-2392-z

Hussein, H. J., & Martinuzzi, R. J. (1996). Energy balance for turbulent flow around a surface mounted cube placed in a channel. *Physics of Fluids*, 8(3), 764–780. https://doi.org/10.1063/1.868860

Inagaki, A., Kanda, M., Ahmad, N. H., Yagi, A., Onodera, N., & Aoki, T. (2017). A numerical study of turbulence statistics and the structure of a spatially-developing boundary layer over a realistic urban geometry. *Boundary-Layer Meteorology*, 164(2), 161–181. https://doi.org/10.1007/s10546-017-0249-y

KONG ET AL. 21 of 23

- Kawaguchi, M., Tamura, T., & Kawai, H. (2019). Analysis of tornado and near-ground turbulence using a hybrid meteorological model/engineering LES method. *International Journal of Heat and Fluid Flow*, 80, 108464. https://doi.org/10.1016/j.ijheatfluidflow.2019.108464
- Kawaguchi, M., Tamura, T., & Mashiko, W. (2020). A numerical investigation of building damage during the 6 May 2012 Tsukuba tornado using hybrid meteorological model/engineering LES method. *Journal of Wind Engineering and Industrial Aerodynamics*, 204, 104254. https://doi. org/10.1016/j.jweia.2020.104254
- Kong, X., Chen, G., Bai, L., Ran, L., Zhang, S., & Meng, Z. (2025). CFD modeling results and related data and codes for plotting of "A Mesoscale-to-LES Modeling of Tornado-like Vortex and Associated Local Strong Winds in Urban Area" [Dataset]. Zenodo. https://doi.org/10.5281/zenodo.15663386
- Kosiba, K. A., Trapp, R. J., & Wurman, J. (2008). An analysis of the axisymmetric three-dimensional low level wind field in a tornado using mobile radar observations. Geophysical Research Letters, 35(5). https://doi.org/10.1029/2007GL031851
- Larousse, A., Martinuzzi, R., & Tropea, C. (1993). Flow around surface-mounted, three-dimensional obstacles. In F. Durst, R. Friedrich, B. E. Launder, F. W. Schmidt, U. Schumann, & J. H. Whitelaw (Eds.), *Turbulent shear flows* (Vol. 8, pp. 127–139). Springer. https://doi.org/10.1007/978-3-642-77674-8_10
- Leonard, B. P. (1979). A stable and accurate convective modelling procedure based on quadratic upstream interpolation. *Computer Methods in Applied Mechanics and Engineering*, 19(1), 59–98. https://doi.org/10.1016/0045-7825(79)90034-3
- Lewellen, D. C. (2012). Effects of topography on tornado dynamics: A simulation study. In *Paper presented at 26th Conference on Severe Local Storms*. American Meteorological Society. Retrieved from https://ams.confex.com/ams/26SLS/webprogram/Paper211460.html
- Lewellen, D. C. (2014). Local roughness effects on tornado dynamics. In *Paper presented at 27th Conference on Severe Local Storms*. American Meteorological Society. Retrieved from https://ams.confex.com/ams/27SLS/webprogram/Paper254357.html
- Li, J., Li, Y., Ping, F., & Tang, J. (2022). A 15-m resolution numerical simulation of a tornado in South China: Structure and vorticity budget of the suction vortices. *Atmospheric Research*, 279, 106390. https://doi.org/10.1016/j.atmosres.2022.106390
- Li, L., Chan, P. W., Deng, T., Yang, H. L., Luo, H. Y., Xia, D., & He, Y. Q. (2021). Review of advances in urban climate study in the Guangdong-Hong Kong-Macau Greater Bay Area, China. Atmospheric Research, 261, 105759. https://doi.org/10.1016/j.atmosres.2021.105759
- Li, S., Jaroszynski, S., Pearse, S., Orf, L., & Clyne, J. (2019). VAPOR: A visualization package tailored to analyze simulation data in Earth system science. Atmosphere, 10(9), 488. https://doi.org/10.3390/atmos10090488
- Lilly, D. K. (1962). On the numerical simulation of buoyant convection. *Tellus*, 14(2), 148–172. https://doi.org/10.1111/j.2153-3490.1962.
- Markowski, P., & Richardson, Y. (2010). Mesoscale meteorology in midlatitudes. John Wiley & Sons. https://doi.org/10.1002/9780470682104 Marshall, T. P. (2002). Tornado Damage Survey at Moore, Oklahoma. Weather and Forecasting, 17(3), 582–598. https://doi.org/10.1175/1520-0434(2002)017<0582:TDSAMO>2.0.CO;2
- Mittal, H., Sharma, A., & Gairola, A. (2018). A review on the study of urban wind at the pedestrian level around buildings. *Journal of Building Engineering*, 18, 154–163. https://doi.org/10.1016/j.jobe.2018.03.006
- Mo, Z., Liu, C. H., & Ho, Y. K. (2021). Roughness sublayer flows over real urban morphology: A wind tunnel study. *Building and Environment*, 188, 107463. https://doi.org/10.1016/j.buildenv.2020.107463
- Muñoz-Esparza, D., Shin, H. H., Sauer, J. A., Steiner, M., Hawbecker, P., Boehnert, J., et al. (2021). Efficient graphics processing unit modeling of street-scale weather effects in support of aerial operations in the urban environment. *AGU Advances*, 2, e2021AV000432. https://doi.org/10.1029/2021AV000432
- Nakayama, H., Takemi, T., & Nagai, H. (2012). Large-eddy simulation of urban boundary-layer flows by generating turbulent inflows from mesoscale meteorological simulations. Atmospheric Science Letters, 13(3), 180–186. https://doi.org/10.1002/asl.377
- Oke, T. R., Mills, G., Christen, A., & Voogt, J. A. (2017). *Urban climates*. Cambridge University Press. https://doi.org/10.1017/9781139016476
 Oliveira, M. I., Xue, M., Roberts, B. J., Wicker, L. J., & Yussouf, N. (2019). Horizontal vortex tubes near a simulated tornado: Three-dimensional structure and kinematics. *Atmosphere*, 10(11), 716. https://doi.org/10.3390/atmos10110716
- Orlanski, I. (1976). A simple boundary condition for unbounded hyperbolic flows. *Journal of Computational Physics*, 21(3), 251–269. https://doi.org/10.1016/0021-9991(76)90023-1
- Overland, J. E., & Walter, B. A. (1981). Gap winds in the Strait of Juan de Fuca. *Monthly Weather Review*, 109(10), 2221–2233. https://doi.org/10.1175/1520-0493(1981)109<2221:GWITSO>2.0.CO;2
- Park, S. B., Baik, J. J., & Lee, S. H. (2015). Impacts of mesoscale wind on turbulent flow and ventilation in a densely built-up urban area. *Journal of Applied Meteorology and Climatology*, 54(4), 811–824. https://doi.org/10.1175/JAMC-D-14-0044.1
- Patankar, S. V. (1980). Numerical heat transfer and fluid flow. CRC Press/Taylor & Francis Group.
- Pazmany, A. L., Mead, J. B., Bluestein, H. B., Snyder, J. C., & Houser, J. B. (2013). A mobile rapid-scanning X-band polarimetric (RaXPol) Doppler radar system. *Journal of Atmospheric and Oceanic Technology*, 30(7), 1398–1413. https://doi.org/10.1175/JTECH-D-12-00166.1
- Ren, C., Yang, R., Cheng, C., Xing, P., Fang, X., Zhang, S., et al. (2018). Creating breathing cities by adopting urban ventilation assessment and wind corridor plan—The implementation in Chinese cities. *Journal of Wind Engineering and Industrial Aerodynamics*, 182, 170–188. https://doi.org/10.1016/j.jweia.2018.09.023
- Satrio, M. A., Bodine, D. J., Reinhart, A. E., Maruyama, T., & Lombardo, F. T. (2020). Understanding how complex terrain impacts tornado dynamics using a suite of high-resolution numerical simulations. *Journal of the Atmospheric Sciences*, 77(10), 3277–3300. https://doi.org/10.1175/JAS-D-19-0321.1
- Sha, W. (2002). Design of the dynamics core for a new-generation numerical model of the local meteorology. *Kaiyo Monthly* (in Japanese), 2, 107–112.
- Sha, W. (2008). Local meteorological model based on LES over the Cartesian coordinate and complex surface. In E. Y. Fujiyoshi (Ed.), Meteorological research note (in Japanese) (Vol. 219, pp. 21–26). Meteorological Society of Japan Press.
- Skamarock, W. C., Klemp, J. B., Dudhia, J., Gill, D. O., Barker, D. M., Duda, M. G., et al. (2008). A description of the advanced research WRF version 3 (No. NCAR/TN-475+STR). University Corporation for Atmospheric Research. https://doi.org/10.5065/D68S4MVH
- Smagorinsky, J. (1963). General circulation experiments with the primitive equations: I. The basic experiment. *Monthly Weather Review*, 91(3), 99–164. https://doi.org/10.1175/1520-0493(1963)091<0099:GCEWTP>2.3.CO;2
- Takemi, T., Yoshida, T., Horiguchi, M., & Vanderbauwhede, W. (2020). Large-eddy-simulation analysis of airflows and strong wind hazards in urban areas. *Urban Climate*, 32, 100625. https://doi.org/10.1016/j.uclim.2020.100625
- Takemi, T., Yoshida, T., Yamasaki, S., & Hase, K. (2019). Quantitative estimation of strong winds in an urban district during Typhoon Jebi (2018) by merging mesoscale meteorological and large-eddy simulations. SOLA, 15, 22–27. https://doi.org/10.2151/sola.2019-005
- Tang, J., Ran, L., Shen, X., & Yan, L. (2019). High-resolution numerical simulation of the EF3 tornadic storm in Foshan city, Guangdong Province. Chinese Journal of Geophysics (in Chinese), 62(11), 4082–4097. https://doi.org/10.6038/cjg2019M0478

KONG ET AL. 22 of 23

- Visualization & Analysis Systems Technologies. (2023). Visualization and Analysis Platform for Ocean, Atmosphere, and Solar Researchers (Version 3.8.0) [Computer software]. UCAR/NCAR Computational and Information Systems Laboratory. https://doi.org/10.5281/zenodo. 7779648
- Wang, W., & Ng, E. (2018). Air ventilation assessment under unstable atmospheric stratification—A comparative study for Hong Kong. Building and Environment, 130, 1–13. https://doi.org/10.1016/j.buildenv.2017.12.018
- Wurman, J., & Alexander, C. R. (2005). The 30 May 1998 Spencer, South Dakota, storm. Part II: Comparison of observed damage and radar-derived winds in the tornadoes. *Monthly Weather Review*, 133(1), 97–119. https://doi.org/10.1175/MWR-2856.1
- Wurman, J., & Gill, S. (2000). Finescale radar observations of the Dimmitt, Texas (2 June 1995), tornado. *Monthly Weather Review*, 128(7), 2135–2164. https://doi.org/10.1175/1520-0493(2000)128<2135:FROOTD>2.0.CO:2
- Wurman, J., Kosiba, K., Robinson, P., & Marshall, T. (2014). The role of multiple-vortex tornado structure in causing storm researcher fatalities. Bulletin of the American Meteorological Society, 95(1), 31–45. https://doi.org/10.1175/BAMS-D-13-00221.1
- Xiang, J., Chen, G., Jiang, P., Wu, N., & Wen, Z. (2019). Fine-scale structures and formation of strong winds over a megacity during a cold surge process. Chinese Journal of Atmospheric Sciences (in Chinese), 43(3), 577–597. https://doi.org/10.3878/j.issn.1006-9895.1805.18140
- Yamazaki, D., Ikeshima, D., Tawatari, R., Yamaguchi, T., O'Loughlin, F., Neal, J. C., et al. (2017). A high-accuracy map of global terrain elevations. Geophysical Research Letters, 44(11), 5844–5853. https://doi.org/10.1002/2017GL072874
- Yang, Z., Sarkar, P., & Hu, H. (2011). An experimental study of a high-rise building model in tornado-like winds. *Journal of Fluids and Structures*, 27(4), 471–486. https://doi.org/10.1016/j.jfluidstructs.2011.02.011
- Yao, D., Meng, Z., & Xue, M. (2019). Genesis, maintenance and demise of a simulated tornado and the evolution of its preceding descending reflectivity core (DRC). Atmosphere. 10(5), 236. https://doi.org/10.3390/atmos10050236
- Zhang, T., Guan, L., Zheng, Y., Chen, C., Cai, K., Li, D., et al. (2020). Damage survey of the 3 July 2019 Kaiyuan tornado in Liaoning Province and its evolution revealed by disaster. *Meteorological Monthly* (in Chinese), 46(5), 603–617. https://doi.org/10.7519/j.issn.1000-0526.2020.
- Zhao, K., Wang, M., Xue, M., Fu, P., Yang, Z., Chen, X., et al. (2017). Doppler radar analysis of a tornadic miniature supercell during the landfall of Typhoon Mujigae (2015) in South China. *Bulletin of the American Meteorological Society*, 98(9), 1821–1831. https://doi.org/10.1175/BAMS-D-15-00301.1
- Zhu, H., & Zhao, Y. (2022). High resolution numerical simulation of an EF4 Tornado in Funing, Jiangsu Province. *Plateau Meteorology* (in Chinese), 41(6), 1599–1614. https://doi.org/10.7522/j.issn.1000-0534.2021.00095

KONG ET AL. 23 of 23